Bifurcation and coalescence of a plethora of homoclinic orbits for a Hamiltonian system

B. Buffoni,* A.R. Champneys† and J.F. Toland

School of Mathematical Sciences,

University of Bath,

Claverton Down,

Bath.

BA2 7AY.

November 8, 1994

*Supported by Swiss National Science Foundation/Royal Society Fellowship. Present address : Scuola Normale Superiore, Pisa.

†Supported by SERC Research Grant. Present address : Department of Engineering Mathematics, University of Bristol.

Abstract

This is a further study of the set of homoclinic solutions (i.e. non-zero solutions asymptotic to 0 as $|x| \to \infty$) of the reversible Hamiltonian system

$$u^{iv} + Pu'' + u - u^2 = 0. \tag{$*$}$$

The present contribution is in three parts.

First, rigorously for $P \leq -2$, it is proved that there is a unique (up to translation) homoclinic solution of (*), that solution is even and in phase space its orbit coincides with the transverse intersection of the global stable and unstable manifolds. When $P = -2$ the origin is a node on its local stable and unstable manifolds and when $P \in (-2, 2)$ it is a focus. Therefore we can infer, rigorously, from the work of Devaney showing Smale horseshoe dynamics on the zero energy set, that there are infinitely many, distinct, infinite families of homoclinic solutions for $P \in (-2, -2+\epsilon)$ for some $\epsilon > 0$. Buffoni has shown globally that there are infinitely many homoclinic solutions for all $P \in (-2, 0]$, based on a different approach due to Champneys and Toland.

Second, numerically, the development of the set of symmetric homoclinic solutions is monitored as P increases from $P = -2$. It is observed that two branches extend from $P = -2$ to $P = +2$ where their amplitudes are found to converge to 0 as $P \nearrow 2$. All other symmetric solution branches are in the form of closed loops, each with a turning point between $P = -2$ and $P = +2$. Numerically it is observed that each such turning point is accompanied by, though not coincident with, the bifurcation of a branch of non-symmetrical homoclinic orbits, which can, in turn, be followed back to $P = -2$.

Finally, heuristic explanations of the numerically observed phenomena are offered in the language of geometric dynamical systems theory. One idea, involving a natural ordering of homoclinic orbits on the stable and unstable manifolds given by the horseshoe dynamics, goes some way to accounting for the observed order (in terms of P-values) of the occurrence of turning points. The near coincidence of turning and asymmetric bifurcation points is explained in terms of the non-transversality of the intersection of the stable and unstable manifolds in the zero energy set on the one hand, and the non-transversality of the intersection of the same manifolds with the symmetric section in $\mathbb{R}^4$, on the other.

Some conjectures based on present understanding are recorded.

The global description of homoclinic orbits for this particular fourth order reversible Hamiltonian system points towards a methodology for more difficult examples. In particular, infinite-dimensional problems, like the solitary water-wave

problem with surface tension where the system is Hamiltonian with a four-dimensional centre manifold, deserve further investigation in the light of these observations.

1 INTRODUCTION

This paper continues a study of reversible Hamiltonian systems with two degrees of freedom, begun in (CHAMPNEYS & TOLAND, 1993), by examining in some detail the theory as it pertains to a particular one-parameter family of problems. The prototype, parametrised by P, can be expressed as a single fourth order ordinary differential equation

$$u^{iv}(t) + Pu''(t) + u(t) - u^2(t) = 0, \quad t \in \mathbb{R}, \tag{1.1}$$

or, equivalently, as Hamilton's equations for the Hamiltonian

$$p_2^2 + p_1 p_2 - \frac{1}{2}(q_2 - \frac{1}{2}(P+2)q_1)^2 + \frac{1}{2}q_1^2 - \frac{1}{3}q_1^3. \tag{1.2}$$

The relation between the two formulations is

$$q_1 = u,\ q_2 = u'' + (1 + \frac{P}{2})u,\ p_1 = \frac{1}{2}(P-2)u' + u''',\ p_2 = u'. \tag{1.3}$$

Note that Equation (1.1) is reversible in the sense that if $(q(t), p(t))$ is a solution to the corresponding Hamiltonian system, then $(q(t), -p(-t))$ is also a solution. In particular, there exists t_0 such that $\dot{q}(t_0) = 0$, and $q(t_0 + t) = q(t_0 - t)$ for all t. Such a solution is said to be symmetric, and $q(t_0)$, $(q(t_0), p(t_0))$ and t_0 are variously called points of symmetry of the solution. The corresponding function u which satisfies (1.1) is even about t_0.

Equation (1.1) arises in (at least) two distinct applications, namely the buckling of a strut on a nonlinear elastic foundation ((HUNT *et al.*, 1989; HUNT & WADEE, 1991)) and as an approximation to travelling solitary water waves in the presence of surface tension ((AMICK & KIRCHGASSNER, 1989; IOOSS & KIRCHGASSNER, 1990)). The one-parameter equation (1.1) is written in a form used in the former application, where t represents the single spatial co-ordinate of the strut, $u(t)$ is its displacement from the trivial equilibrium state $u \equiv 0$ and P represents the strength of a compressive load which is critical at $P = 2$. For water waves, $u(t)$ in some sense describes the negative displacement of the free surface in a co-ordinate frame that is moving at the wave speed. Here one should consider P as a dimensionless combination of the Bond and Froude numbers.

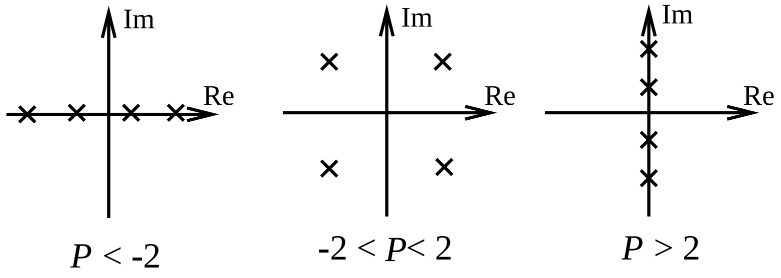

Figure 1: *Eigenvalues of the linearised problem*

We are concerned exclusively with the so-called *homoclinic* boundary condition, namely that

$$u^{(k)}(t) \to 0 \text{ as } |t| \to \infty, \quad k = 0, 1, 2, 3 \tag{1.4}$$

or, equivalently,

$$(q(t), p(t)) \to 0 \text{ in } \mathbb{R}^2 \times \mathbb{R}^2 \text{ as } |t| \to \infty. \tag{1.5}$$

Such orbits said to be homoclinic to the zero equilibrium and correspond to *localised* post-buckling modes of the strut or to *solitary* water waves. In what follows, "homoclinic" shall always be taken to mean "homoclinic to zero".

The problem linearised at zero is

$$u^{iv} + Pu'' + u = 0$$

and the corresponding characteristic equation is

$$\chi^4 + P\chi^2 + 1 = 0, \ \chi \in \mathbb{C}. \tag{1.6}$$

It is easily checked that when $P < -2$ there are four distinct real solutions $\pm\lambda_1, \pm\lambda_2, \lambda_1 < \lambda_2 < 0$; when $-2 < P < 2$ there are four distinct complex solutions $\pm(\lambda \pm i\mu)$; when $P > 2$ there are four distinct imaginary solutions $\pm i\mu_1, \pm i\mu_2, \mu_1 < \mu_2 < 0$ (see Figure 1).

When $P < 2$ the stable and unstable manifolds are two dimensional; when $P < -2$ the origin is a node on each, whereas when $-2 < P < 2$ it is a focus. Therefore when $P < -2$ we say 0 is a saddle-node, when $-2 < P < 2$, it is a saddle-focus and when $P > 2$, we say 0 is a centre.

The purpose of the present paper is to investigate the set of homoclinic solutions of (1.1), both symmetric and asymmetric, for various values of P.

1.1 The Main Results

It is known ((AMICK & TOLAND, 1992)) that for $P \leq -2$ there is a unique non-zero symmetric homoclinic solution. That is, for each $P \leq -2$, in the set of non-zero even functions there is one and only one homoclinic solution of (1.1). In Section 2 we extend this result and show that the even solution is the unique solution among all functions which satisfy the homoclinic boundary conditions. In addition, for $P \leq -2$, we show rigorously that the orbit in phase space of this solution is the transverse intersection of the stable and unstable manifolds of 0 (transversality here refers to transversality within the zero level set of (1.2)). Further, when $P = -2$, the unique non-zero solution has the property that

$$u(t)/te^{-t} \to \alpha \neq 0 \text{ as } t \to \infty.$$

Note that $\chi = -1$ is a double root of the characteristic equation when $P = -2$.

The results of Section 2 provide a complete proof that the hypotheses at $P = -2$, required for the theory of (CHAMPNEYS & TOLAND, 1993), hold in this prototypical problem. In particular, Theorem 4.4 (CHAMPNEYS & TOLAND, 1993) holds in this case, and there follows at once the existence of infinitely many, *bi-modal* symmetric homoclinic orbits for $P \in (-2, -2+\epsilon)$ for some $\epsilon > 0$. In particular, for each $\ell \in \mathbb{N}$ there is an orbit whose graph $\{u(t) : t \in \mathbb{R}\}$ has the following features:

(i) exponentially decaying oscillatory tails as $t \to \pm\infty$;

(ii) two large local maxima;

(iii) in the interval between these large local maxima there are $\ell/2$ small oscillations (in a sense made precise in Section 3 below) with the symmetric point occurring in the middle of this interval;

(iv) as $P \downarrow -2$ the amplitudes of the large local maxima do not diminish (rather the profiles of both local maxima converge uniformly on compact intervals centred on the local maxima to the profile of the unique solution which exists at $P = -2$);

(v) the amplitudes of the small oscillations between the large local maxima tend to 0 as $P \downarrow -2$;

(vi) as $P \downarrow -2$ the horizontal distance (in t) between the t-values at which the large maximum values occur tend to infinity.

Previous numerical results ((CHAMPNEYS, 1994; CHAMPNEYS & SPENCE, 1993; CHAMPNEYS & TOLAND, 1993)) suggest that, in fact, there exist many more homoclinic orbits for $P \in (-2, -2+\epsilon)$, which are *multi-modal*. That is, they obey properties similar to (i)–(vi) above, but with $n > 2$ large local maxima and $l_k \in \mathbb{N}$, $k = 1, \ldots, n-1$, small amplitude oscillations in the kth interval between these large local maxima.

In Section 3 we review and extend these numerical results (see Section 1.3 for a brief description of the numerical methods used), and discuss them in the light of two approaches that prove the existence of homoclinic solutions for each fixed P in some interval $(-2, -2+\epsilon)$. The first of these approaches, which goes back to Devaney (DEVANEY, 1976) (see also Wiggins (WIGGINS, 1988), page 275) and has been amplified more recently by Belyakov and Šil'nikov (BELYAKOV & ŠIL'NIKOV, 1990), is relevant here for the following reason. At $P = -2$ there is a unique homoclinic orbit which is the transverse intersection of the global stable and unstable manifolds. For P slightly larger than -2 the transversality persists and at the same time the zero equilibrium becomes a saddle-focus. In this setting Devaney (DEVANEY, 1976) found a Smale horseshoe in the dynamics restricted to the zero energy set. The second approach, which is more recent and conceptually different, involves a detailed study of paths in configuration space (q-space) of orbits with zero energy (see ((HOFER & TOLAND, 1984; TOLAND, 1986)). It was this approach that was used to prove the results described above on the existence of primary and bi-modal orbits ((AMICK & TOLAND, 1992; BUFFONI, 1993a; BUFFONI & TOLAND, n.d.; CHAMPNEYS & TOLAND, 1993)). In Section 3.1, we propose a classification of all possible multi-modal orbits according to the number of times their paths in configuration space encircle the origin during maximal compact time intervals when they are in a fixed small neighbourhood of 0. Hence a multi-modal orbit is labelled by a symbol sequence

$$\mathbf{n}(\ell_1, \ldots, \ell_{n-1})$$

where $\mathbf{n}$ is the *modality*, i.e. the number of large local maxima, and ℓ_k is twice the number of encirclings of the origin of configuration space between consecutive large local maxima (see Section 3.1 for a more precise definition). In Section 3.3 it is conjectured that, for each $P \in (-2, -2+\epsilon)$, there exits a homoclinic orbit corresponding to each possible label. An ordering of these orbits in the unstable manifold is also motivated. While these are still only conjectures, it is shown how they are consistent with Devaney's theory. Also, the numerical evidence (Section 3.2) strongly suggests these conjectures are not just local, but hold for ϵ as large as 3.5. Note that the set of homoclinic orbits thus described contains both symmetric and asymmetric solutions.

Sections 4–6 are concerned with results for $P > -2+\epsilon$. Rigourous theory for $P > -2$ is in a less satisfactory state than that for $P \leq -2$ and, given the results presented in Sections 4–6, it seems unlikely that hard analysis can shed much light on the detailed structure of the global solution set. (Look ahead to Figure 24 for a flavour of the complexities involved.) We begin by first mentioning what is known rigorously when $P > -2+\epsilon$.

Buffoni (BUFFONI, 1993b) has used the Mountain Pass Lemma to prove that for all $P \in (-\infty, 2)$ there is at least one non-trivial solution, which is unique when $P \leq -2$ (Section 2). Note that, if it is known that this orbit is transversal in the sense of Section 2 and $P \in (-2,2)$, Devaney's theory implies the existence of infinitely many homoclinic orbits for that $P \in (-2,2)$. Other work has shown that, for all $P \in (-2,0]$, there is at least one uni-modal orbit ((BUFFONI & TOLAND, n.d.) or (AMICK & TOLAND, 1992)) and an m-modal orbit for all m ((BUFFONI, 1993a)). From the work of Iooss and Pérouème (IOOSS & PEROUEME, 1993) (and Mielke (MIELKE, 1991), see also the asymptotic analysis in (HUNT *et al.*, 1989; HUNT & WADEE, 1991)) we know that for $P < 2$ and close to 2, there are at least two even solutions with amplitudes tending to 0 as $P \to +2$.

Our purpose in Section 4 is to give an informal discussion of what generically may happen to a branch of homoclinic orbits as a parameter is varied for systems, such as (1.1), which are both reversible and Hamiltonian. A broader concept of reversibility is considered and symmetric and asymmetric orbits are treated separately. For symmetric orbits, the discussion was motivated by numerical results (first presented in (CHAMPNEYS & SPENCE, 1993; CHAMPNEYS & TOLAND, 1993) and extended here in Section 5) that only two of all the possible branches continues through the range $P \in (-2,2)$. Upon increasing P, all other branches are found to reach a turning point at a critical value of $P < 2$ beyond which the branch ceases to exist. If the value of P is decreased from this critical value we can return along a different branch emerging at $P = -2$ at an orbit labelled by a different symbol sequence (indeed, of a different modality) from that where we began the experiment close to -2. Thus the numerical evidence suggests that most symmetric orbits lie on loops in a bifurcation diagram (see Figure 24). At the turning points, branches of symmetric orbits which were identified for P close to -2 as being labelled by different sequences of symbols are said to *coalesce*. In Section 4, this phenomenon is identified with a non-transverse intersection in $\mathbb{R}^4$ of the two-dimensional stable manifold and the symmetric section $\{u' = u''' = 0\}$.

Then we turn to the possibility of asymmetric homoclinic orbits. Here the numerical evidence, surprisingly, suggests that coalescence of symmetric orbits and bifurcation of asymmetric orbits often go hand-in-hand. In Section 4 the bifurcation, from a one parameter curve of symmetric homoclinic orbits, of a curve of asymmetric orbits is identified with the following situation at symmetric points on the critical orbit where bifurcation occurs.

(i) The two-dimensional stable manifold and the symmetric section intersect transversally in $\mathbb{R}^4$; this ensures the persistence of the symmetric orbits as parameters are varied.

(ii) The two-dimensional stable and unstable manifolds do not intersect transversally, which allows the asymmetric bifurcation to be forced by (i) in generic situations.

The bifurcations points of asymmetric homoclinic solutions are found numerically to be remarkably close to, but clearly distinct from, the turning points of branches of symmetric orbits discussed above. This phenomenon is interpreted as reflecting the tentacle-like geometry of the stable and unstable manifolds in a Poincaré section (see Figure 17).

It is also argued in Section 4, that, as an alternative to bifurcating from a symmetric orbit, another possible fate of a branch of asymmetric homoclinic orbits upon varying P is that it coalesces with an asymmetric homoclinic orbit with a different symbol sequence. This coalescence is caused by a non-transverse intersection of the stable and unstable manifolds away from the symmetric section.

Section 5 is devoted to a thorough numerical investigation of the global properties (i.e. bifurcation and coalescence) of branches of homoclinic orbits for $P \in (-2, 2)$. Again symmetric and asymmetric orbits are treated separately. The results for asymmetric orbits are completely new, whereas those for symmetric orbits extend the results first presented in ((CHAMPNEYS & TOLAND, 1993)). The focus here is a systematic attempt to uncover rules that determine which pairs of orbits coalesce (i.e. relations between the two symbol sequences that label, near $P = -2$, two orbits that are connected by a loop). A related question is the ordering with respect to P of specific coalescences.

In Section 6 some effort is expended in trying to establish a theoretical basis for the numerical observations made in Section 5. Only symmetric homoclinic orbits are treated, but even for this restricted problem, precise results seem hard. Nevertheless, we are able to establish, based on the conjectures in Section 3, certain exclusion principles which say that orbits of certain types do not coalesce, whereas others cannot coalesce unless certain other orbits coalesce for smaller P-values.

For related results on multiplicity of homoclinic solutions, see Section 1.3 ((CHAMPNEYS & TOLAND, 1993)) and the references therein.

1.2 Numerical Methods

Before embarking on the investigation set out above we give a brief account of the numerical methods used to compute branches of homoclinic orbits. There are two stages; first the computation of an orbit at a fixed parameter value and then the continuation of the orbit as a parameter is varied. Note that a homoclinic solution satisfies a boundary-value problem on an infinite time interval. The key to performing both steps mentioned above is therefore to write a suitable boundary-value problem that approximates the full problem, but on a finite time interval. The two stages of computation are then two different approaches to solving this approximate boundary-value problem. For the boundary-value problems approximating (1.1),(1.4) we have used shooting methods to generate initial solutions (see (CHAMPNEYS & SPENCE, 1993; KUZNETSOV, 1990)) and the code AUTO for continuation (see (DOEDEL *et al.*, 1991a; DOEDEL *et al.*, 1991b)). The reader is referred to these cited works for more details on numerical methods. We confine discussion here to the approximating boundary-value problems.

Approximate boundary-value problems for generic homoclinic orbits (which excludes the cases of homoclinic orbits in Hamiltonian systems or symmetric homoclinic orbits in reversible systems) have been proposed by Beyn ((BEYN, 1990)) and Friedman and Doedel ((FRIEDMAN & DOEDEL, 1991)) in the broader context of computing heteroclinic connections between hyperbolic equilibria. Here, to approximate the problem

$$\dot{x} = f(x, \lambda), \quad x \in \mathbb{R}^N,\ \lambda \in \mathbb{R}, \tag{1.7}$$

$$x \to 0 \text{ as } t \to \pm\infty, \tag{1.8}$$

one truncates to a sufficiently large, finite time interval $t \in [-T, T]$ and solves (1.7) subject to

$$L_s(\lambda)x(-T) = 0,\ L_u(\lambda)x(T) = 0,\ \phi(x(t), \lambda) = 0, \tag{1.9}$$

where $L_{s,u}(\lambda)$ are projection operators onto the stable and unstable eigenspaces of $Df(0, \lambda)$, and ϕ is a scalar function used to fix the phase.

Given a judicious choice of phase condition (e.g. (DOEDEL, 1981)), (1.7),(1.9) is a well-posed problem only if the origin is hyperbolic and homoclinic orbits exist in co-dimension-one subsets of parameter space (see (BEYN, 1990; FRIEDMAN & DOEDEL, 1991), where there are also results on the convergence of solutions of (1.7),(1.9) to solutions of (1.7),(1.8) as T is increased). However, homoclinic orbits to hyperbolic equilibria in Hamiltonian systems typically persist as parameters are varied and so (1.7),(1.9) is not a well-posed problem in this sense for Hamiltonial systems. However, Beyn ((BEYN, 1990)) shows that if a Hamiltonian system

$$\dot{q} = \frac{\partial H(q,p)}{\partial p}, \quad \dot{p} = -\frac{\partial H(q,p)}{\partial q}, \quad (q,p) \in \mathbb{R}^n \times \mathbb{R}^n \tag{1.10}$$

possesses a homoclinic orbit to 0 then the boundary value problem (1.7),(1.9) will be well posed if one takes $x = (q, p)$, $N = 2n$ and

$$f = \left(\frac{\partial H(q,p)}{\partial p} + \lambda \frac{\partial H(q,p)}{\partial q}, -\frac{\partial H(q,p)}{\partial q} + \lambda \frac{\partial H(q,p)}{\partial p} \right)^T. \tag{1.11}$$

This extended problem is well-posed and has a regular solution with $\lambda \approx 0$, which is a good approximation to the homoclinic solution of (1.10).

Alternatively, a numerical method for symmetric homoclinic orbits in reversible systems was proposed in (CHAMPNEYS & SPENCE, 1993). Due to the symmetry, one need only solve an approximation to (1.7),(1.8) on the half-interval $[-T, 0]$, with a right-hand boundary condition that places the solution in the symmetric section Σ ($\{u' = u''' = 0\}$ for the present problem). Thus one solves (1.7) with boundary conditions

$$L_s x(-T) = 0, \quad x(0) \in \Sigma. \tag{1.12}$$

Using this approach, one does not need a phase condition, because the phase is fixed by the right-hand boundary condition. Therefore, the parameter λ need no longer be treated as an unknown, and (1.7),(1.12) will apply to the computation of homoclinic orbits that persist as parameters are varied.

To compute asymmetric homoclinic orbits, we have used the full projection boundary conditions (1.9) applied to the extended system (1.11). For symmetric orbits, however, it is advantageous to use the symmetric section boundary condition (1.12), because this halves the interval of computation and leads to a more robust shooting method (see (CHAMPNEYS & SPENCE, 1994)). Note, however, that using the latter method, a continuation code such as AUTO will be unable to detect bifurcations of asymmetric homoclinic orbits from symmetric ones.

2 ANALYTIC PROPERTIES OF THE PRIMARY ORBIT

The purpose of this Section is a rigorous proof of uniqueness of homoclinic orbits, the transverse intersection of stable and unstable manifolds for $P \leq -2$ and the genericity of the homoclinic orbit at $P = -2$ in the sense of (CHAMPNEYS & TOLAND, 1993).

2.1 Transversality

The equation under consideration is

$$u^{iv}(t) + Pu''(t) + u(t) - u^2(t) = 0, \;\; P \leq -2. \tag{2.1}$$

The following application of the maximum principle is the key.

Theorem 2.1 *Let* $p + p^{-1} = -P, \;\; p \in (0,1]$. *Suppose that* u *and* v *are solutions of (2.1) on* $[0, \infty)$ *with*

$$\begin{aligned}
&u(0) \geq v(0) > 0, u'(0) \geq v'(0),\\
&u''(0) - pu(0) \geq v''(0) - pv(0), \quad u'''(0) - pu'(0) \geq v'''(0) - pv'(0).
\end{aligned}$$

If $v(t) \geq 0, \;\; t = [0, \infty)$ *then* $u \equiv v$ *or* $u(t) \to \infty$ *as* $t \to \infty$.

Proof. Suppose $u \not\equiv v$. Then let k be the smallest derivative for which $u^{(k)}(0) \neq v^{(k)}(0)$. Then $k \in \{0, 1, 2, 3\}$ exists and, by our hypotheses, $u^{(k)}(0) > v^{(k)}(0)$. Hence there exists $\sigma > 0$ such that

$$u(t) > v(t) \geq 0 \text{ on } (0, \sigma),$$

since $v(t) \geq 0$ is given. Now let

$$\phi(t) = u''(t) - pu(t) \text{ and } \psi(t) = v''(t) - pv(t).$$

Then

$$\phi(0) - \psi(0) \geq 0, \quad \phi'(0) - \psi'(0) \geq 0$$

and

$$(\phi - \psi)''(t) - p^{-1}(\phi - \psi)(t) = u^2(t) - v^2(t) > 0 \text{ on } (0, \sigma).$$

It is immediate that

$$\phi(t) - \psi(t) > 0 \text{ on } (0, \sigma).$$

This is to say

$$(u - v)''(t) - p(u - v)(t) > 0 \text{ on } (0, \sigma),$$

and, by hypothesis,

$$(u - v)(0) \geq 0, \quad (u - v)'(0) \geq 0.$$

Therefore

$$u(t) > v(t) \geq 0 \text{ on } (0, \sigma]$$

whence

$$u(t)^2 > v(t)^2 \geq 0 \text{ on } (0, \sigma].$$

Therefore

$$\sup\{\sigma : u(t) > v(t) \geq 0 : t \in [0, \sigma)\} = +\infty,$$

$$(\phi - \psi)''(t) - p^{-1}(\phi - \psi)(t) > 0, \quad t \in [0, \infty),$$
$$(u - v)''(t) - p(u - v)(t) > 0, \quad t \in [0, \infty).$$

Since $u \not\equiv v$ it is immediate that

$$(u - v)(t) \to \infty \text{ as } t \to \infty.$$

Since $v(t) \geq 0$ it follows that $u(t) \to \infty$ as $t \to \infty$.

$\square$

Theorem 2.2 *Suppose that $v \not\equiv 0$ is a solution of (2.1) with $v(0) \geq 0 \geq v''(0)$ and $v(t) \to 0$ as $t \to \infty$. Then $v(t) > 0, \quad t \in (0, \infty)$.*

Proof. Let $\psi(t) = v''(t) - pv(t), \quad t \geq 0$. Then

$$\psi(0) \leq 0, \quad \liminf_{t\to\infty} \psi(t) \leq 0,$$

and

$$\psi''(t) - p^{-1}\psi(t) = v^2(t) \geq 0, \quad t \geq 0.$$

By the maximum principle ψ is non-positive and hence

$$v''(t) - pv(t) = \psi(t) \leq 0, \quad t \geq 0$$

$$v(0) \geq 0, \quad v(t) \to 0 \text{ as } v \not\equiv 0.$$

Therefore $v(t) > 0, \quad t > 0$ if $v \not\equiv 0$.

$\square$

Theorem 2.3 *Suppose that v is a solution of (2.1) with*

$$v''(0) < 0 < v(0) \textit{ and } v'(0) = v'''(0) = 0$$

such that $v(t) \to 0$ as $t \to \infty$. Suppose also that u is a solution of (2.1) with

$$k\epsilon \geq u''(0) - v''(0) \geq (1+\alpha)p(u(0) - v(0)) \geq (1+\alpha)p\epsilon$$

and

$$|u'(0)| + |u'''(0)| \leq \beta\epsilon^2,$$

where $k, \alpha, \beta > 0$ are constants. Then, for $\epsilon > 0$ sufficiently small, $u(t) \not\to 0$ as $t \mapsto \infty$.

Proof. Since the solution v exists on $[0, \infty)$ there exists $\epsilon_0 > 0$ such that if $\epsilon \in (0, \epsilon_0)$ then the function u and its derivatives of all orders exist and are bounded on $[0, 1]$, independent of $\epsilon \in (0, \epsilon_0)$. In consequence, by Taylor's theorem, for $t \in [0, 1]$

$$\begin{aligned}
u(t) - v(t) &\geq u(0) - v(0) + (u'(0) - v'(0))t - Mt^2 \\
&\geq \epsilon - \beta\epsilon^2 t - Mt^2 \\
u'(t) - v'(t) &\geq u'(0) - v'(0) + (u''(0) - v''(0))t + \frac{1}{2}(u'''(0) - v'''(0))t^2 - Mt^3 \\
&\geq -\beta\epsilon^2 + (1+\alpha)p\epsilon t - \frac{1}{2}\beta\epsilon^2 t^2 - Mt^3;
\end{aligned}$$

$$
\begin{aligned}
(u''-pu)(t) &- (v''-pv)(t) \geq (u''-pu)(0)-(v''-pv)(0)\\
&+ \{(u'''-pu')(0)-(v'''-pv')(0)\}t - Mt^2\\
&\geq \alpha p\epsilon - \beta\epsilon^2 t - Mt^2;\\
(u'''-pu')(t) &- (v'''-pv')(t) = (u'''-pu')(0)-(v'''-pv')(0)\\
&+ \{(u^{iv}-pu'')(0)-(v^{iv}-pv'')(0)\}t + \frac{1}{2}\{(u^{v}-pu''')(0)-(v^{v}-pv''')(0)\}t^2 - Mt^3\\
&\geq -\beta\epsilon^2 + \alpha\epsilon t - \gamma\epsilon^2 t^2 - Mt^3, \quad \text{for some } \gamma \geq 0 \text{ and } M \geq 0.
\end{aligned}
$$

Here we have used the following facts: since $u(0) > v(0) > 0$, (2.1) gives

$$
\begin{aligned}
(u^{iv}-pu'')(0) &= p^{-1}(u''(0)-pu(0)) + u^2(0)\\
&\geq p^{-1}(v''(0)-pv(0)) + \alpha(u(0)-v(0)) + u^2(0)\\
&\geq (p^{-1}v''-v)(0) + \alpha\epsilon + u^2(0), \text{ by hypothesis}\\
&= (v^{iv}-pv'')(0) + \alpha\epsilon + (u^2(0)-v^2(0))\\
&> (v^{iv}-pv'')(0) + \alpha\epsilon;
\end{aligned}
$$

$v^v(0) = 0$ (by symmetry) and $|u^v(0)| \leq \gamma\epsilon^2$, by (2.1) and the boundary conditions.

Hence if $\hat{\alpha} = \min\{1, \alpha p\} > 0$ then

$$u(t)-v(t) \geq 0 \text{ and } (u''-pu)(t)-(v''-pv)(t) > 0 \text{ on } [0, \Gamma(\epsilon)]$$

where

$$\Gamma(\epsilon) = \sqrt{\epsilon}\left\{\sqrt{\frac{\hat{\alpha}}{M}} - \frac{\beta\epsilon^{3/2}}{2M}\right\}.$$

Let $\tau(\epsilon) = \epsilon^{2/3}$. Then $\tau(\epsilon) \in [0, \Gamma(\epsilon)] \cap [0,1]$ for all $\epsilon > 0$ sufficiently small. Now

$$(u'''-pu')(\tau(\epsilon)) - (v'''-pv')(\tau(\epsilon)) \geq -\beta\epsilon^2 + \alpha\epsilon^{5/3} - \gamma\epsilon^{10/3} - M\epsilon^2 > 0$$

for $\epsilon > 0$ sufficiently small and

$$(u'-v')(\tau(\epsilon)) \geq -\beta\epsilon^2 + (1+\alpha)p\epsilon^{5/3} - \frac{1}{2}\beta^2\epsilon^{10/3} - M\epsilon^2 > 0$$

for $\epsilon > 0$ sufficiently small.

By Theorem 2.2 and the present hypotheses $v(t) > 0$ for all $t \geq \tau(\epsilon)$. Hence, by Theorem 2.1, $u(t) \not\to 0$ as $t \to \infty$.

This completes the proof.

$\square$

Theorem 2.4 *Let v be the solution of (2.1) identified in Theorem 2.3. Suppose that u is a solution of (2.1) with*

$$4\alpha\epsilon \geq u'''(0) - pu'(0) \geq u'(0) \geq \alpha\epsilon$$
$$|u(0) - v(0)| + |u''(0) - v''(0)| \leq \beta\epsilon^2$$

where $\alpha, \beta > 0$ are constants. Then for $\epsilon > 0$ sufficiently small $u(t) \not\to 0$ as $t \to \infty$.

Proof. We proceed as in the proof of Theorem 2.3 and find, by Taylor's Theorem, that for some $M \geq 0$ and $K \geq 0$ and $t \in [0,1]$,

$$\begin{aligned}
u(t) - v(t) &\geq -\beta\epsilon^2 + \alpha\epsilon t - \frac{1}{2}\beta\epsilon^2 t^2 - Mt^3, \\
u'(t) - v'(t) &\geq \alpha\epsilon - \beta\epsilon^2 t - Mt^2, \\
(u'' - pu)(t) - (v'' - pv)(t) &\geq -2\beta\epsilon^2 + \alpha\epsilon t - K\epsilon^2 t^2 - Mt^3, \\
(u''' - pu')(t) - (v''' - v')(t) &\geq \alpha\epsilon - K\epsilon^2 t - Mt^2.
\end{aligned}$$

Let

$$\Gamma(\epsilon) = \sqrt{\epsilon}\left\{\sqrt{\frac{\alpha}{M}} - \frac{\hat{\alpha}}{2M}\epsilon^{3/2}\right\}, \quad \hat{\alpha} = \min\{\beta, K\}.$$

Then, on $[0, \Gamma(\epsilon)]$,

$$u'(t) - v'(t) \geq 0 \text{ and } (u''' - pu')(t) - (v''' - pv')(t) \geq 0.$$

If $\tau(\epsilon) = \epsilon^{2/3}$ then $\tau(\epsilon) \in [0,1]\,[0, \Gamma(\epsilon)]$ for $\epsilon > 0$ sufficiently small and

$$\begin{aligned}
u(\tau(\epsilon)) - v(\tau(\epsilon)) &\geq -\beta\epsilon^2 + \alpha\epsilon^{5/3} - \frac{1}{2}\beta\epsilon^{10/3} - M\epsilon^2 > 0 \\
(u'' - pu)(\tau(\epsilon)) - (v'' - pv)(\tau(\epsilon)) &\geq -2\beta\epsilon^2 + \alpha\epsilon^{5/3} - K\epsilon^{10/3} - M\epsilon^2 > 0
\end{aligned}$$

for $\epsilon > 0$ sufficiently small. Since $v \geq 0$ on $[\tau(\epsilon), \infty)$ the result is now immediate by Theorem 2.1.

q.e.d.

Remark. One particular consequence of the preceding discussion is that there is a unique even solution of (2.1) which tends to 0 as $t \to \infty$. (See (AMICK & TOLAND,

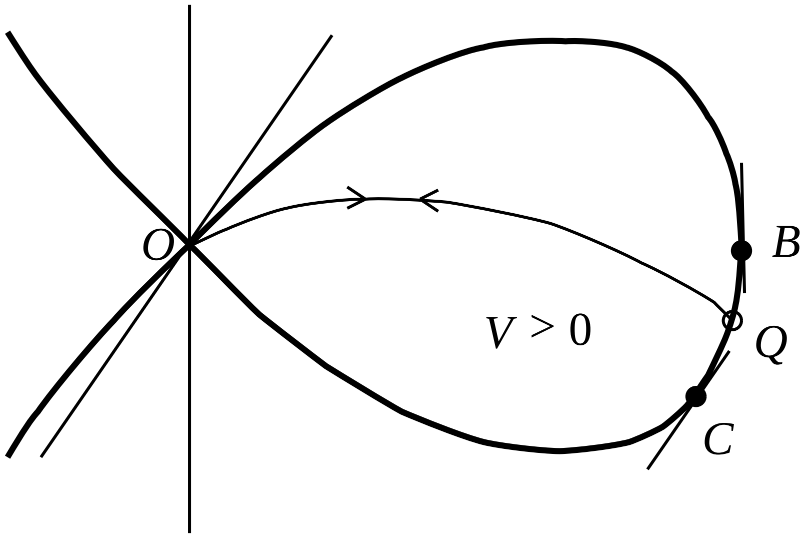

Figure 2: *The path of the symmetric homoclinic orbit in the vv'' plane for $P \leq -2$*

1992) for further details.) Figure 2 illustrates the position of $(v(0), v''(0))$ relative to the level set

$$\mathcal{C} = \{(v, v'') : \frac{1}{2}v''^2 = \frac{1}{2}v^2 - \frac{1}{3}v^3\}.$$

It is shown in (AMICK & TOLAND, 1992), Theorem 3, that if v is an even homoclinic solution of (2.1), i.e. if $v'(0) = v'''(0) = 0$, then $(v(0), v''(0))$ lies on $\mathcal{C}$ between C and B in Figure 2. Here the tangent to $\mathcal{C}$ at B is vertical and at C it has slope $-P/2$
Note, in particular, the tangent to $\mathcal{C}$ at $Q = (v(0), v''(0))$, when $P \leq -2$, has slope $(1+\eta)$ for some $\eta > 0$. Therefore

$$\frac{v^2(0) - v(0)}{-v''(0)} = 1 + \eta > 1. \tag{2.2}$$

Now, by assumption,

$$(v(0), v'(0), v''(0), v'''(0)) \in S, \quad v'(0) = v'''(0) = 0,$$

where S is the stable manifold of the zero equilibrium of (2.1), and

$$(v'(v''' + \frac{P}{2}v') + \frac{1}{2}v^2 - \frac{1}{3}v^3 - \frac{1}{2}v''^2)(t) = 0, \quad t \in \mathbb{R}.$$

If we use (u, u', u'', u''') to denote elements of the phase space of (2.1) then the tangent space to the zero energy manifold at the point $(v(0), 0, v''(0), 0)$ is

$$(v(0) - v^2(0),\ 0, -v''(0), 0)^{\perp} \subset \mathbb{R}^4.$$

Now the tangent spaces to the two-dimensional stable and unstable manifolds at this point both contain the vector

$$(0, v''(0), 0, -Pv''(0) - v(0) + v(0)^2)$$

because of the differential equation.

Now let us suppose, seeking a contradiction, that these stable and unstable manifolds do not intersect transversally in the zero energy set. Then their tangent spaces coincide in a two-dimensional space, T say. Then $(\alpha, \beta, \gamma, \delta)$ lies in the stable manifold if and only if $(\alpha, -\beta, \gamma, -\delta)$ lies in the unstable manifold because (2.1) is reversible. It then follows that

$$(\alpha, \beta, \gamma, \delta) \in T \text{ if and only if } (\alpha, -\beta, \gamma, -\delta) \in T.$$

There are therefore only two possibilities

$$\begin{aligned}
\text{(I) } T &= \{(0, a, 0, b) : a, b \in \mathbb{R}\} && (2.3)\\
\text{(II) } T &= \{(-av''(0),\ bv''(0), a(v^2(0) - v(0)), b(-Pv''(0) - v(0) + v^2(0)) : \\
& \qquad a, b \in \mathbb{R}\}. && (2.4)
\end{aligned}$$

If (I) is the case, let $a = 1,\ b = 3$ and consider the point (u, u', u'', u''') on the stable manifold given by

$$(u, u', u'', u''')(0) = (v(0) + O(\epsilon^2), \epsilon + O(\epsilon^2), v''(0) + O(\epsilon^2), 3\epsilon + O(\epsilon^2)).$$

Then the hypotheses of Theorem 2.4 are satisfied for $\epsilon > 0$ sufficiently small. Hence $u(t) \not\to 0$ as $t \to \infty$ which contradicts the claim that (u, u', u'', u''') lies on the stable manifold. Thus (I) is false.

Now suppose (II) and let $a = 1, b = 0$. Then there exists a point (u, u', u'', u''') on the stable manifold in the form

$$(v(0) - \epsilon v''(0) + O(\epsilon^2),\ O(\epsilon^2),\ v''(0) + \epsilon(v^2(0) - v(0)) + O(\epsilon^2), O(\epsilon^2)).$$

Now

$$(u - v)(0) = -\epsilon v''(0) + O(\epsilon^2)$$

and, from (2.2),

$$\begin{aligned}
(u'' - v'')(0) &= \epsilon(v^2(0) - v(0)) + O(\epsilon^2)\\
&\geq -\epsilon(1 + \eta)v''(0) + O(\epsilon^2)\\
&\geq (1 + \eta)(u - v)(0) + O(\epsilon^2).
\end{aligned}$$

If we take $\alpha = \eta/2$ in Theorem 2.3, we find that for $\epsilon > 0$ sufficiently small its hypotheses are satisfied since $p \in (0,1]$. Hence $u(t) \not\to 0$ as $t \to \infty$ which violates the claim that (u, u', u'', u''') lies on the stable manifold. Thus (II) is false.

The conclusion is that *the stable and unstable manifolds of* (2.1) *intersect transversally at* $(v(0), 0, v''(0), 0)$.

2.2 Uniqueness

It was remarked earlier that there is a unique even homoclinic orbit for $P \leq -2$. We now show that, in fact, all homoclinic orbits are even and thus there is only one homoclinic orbit.

Theorem 2.5 *If $P \leq -2$, every solution of (2.1) with the property that $u(t) \to 0$ as $|t| \to \infty$, $u \not\equiv 0$, is even about some t_0. In particular the homoclinic solution of (2.1) is, up to translation, unique.*

Proof. Suppose that u is a solution of (2.1). Let $\phi = u'' - pu$. Then

$$\phi'' - p^{-1}\phi = u^2 \geq 0 \text{ on } \mathbb{R}.$$

Since $u \to 0$ as $|t| \to \infty$, we infer that

$$\liminf_{t \to \pm\infty} \phi = \liminf_{t \to \pm\infty} u'' - pu \leq 0.$$

Hence $\phi \leq 0$ on $\mathbb{R}$, by the maximum principle. But it follows that $u > 0$ on $\mathbb{R}$ since

$$u'' - pu \leq 0 \text{ on } \mathbb{R} \text{ and } |u(t)| \to 0 \text{ as } |t| \to \infty.$$

Now let the origin of t be chosen so that $u'(0) = 0$ (such a point exists). Suppose that $u'''(0) \neq 0$. Let $v(t) = u(-t)$. By reversibility v is a homoclinic solution of (2.1) and $v'(0) = 0$, $v'''(0) = -u'''(0)$. We may suppose $u'''(0) > 0 > v'''(0)$. Then

$$\begin{aligned} &u(0) = v(0), \quad u''(0) = v''(0) \\ &u''(0) - pu(0) = v''(0) - pv(0) \\ &u'''(0) - pu'(0) > v'''(0) - pv'(0). \end{aligned}$$

By Theorem (2.1) $u(t) \to \infty$ as $t \to \infty$ which contradicts the hypothesis. Hence $u'''(0) = 0$ and u is symmetric. The uniqueness of even solutions is proved in (AMICK & TOLAND, 1992), Theorems 2 and 3.

□

2.3 Asymptotic behaviour when $P = -2$

To complete the discussion of even homoclinic orbits, we study asymptotic behaviour as $t \to \infty$ when $P = -2$. The equation, linearised about equilibrium, is then

$$w^{iv} - 2w'' + w = 0$$

and the characteristic equation

$$(\chi^4 - 2\chi^2 + 1) = 0$$

has double roots $\chi = +1$ and $\chi = -1$. Therefore the stable manifold theorem says that if u is a solution of (2.1) which tends to 0 as $t \to \infty$ then

$$\begin{aligned}
u(t) &= ae^{-t} + bte^{-t} + o(e^{-t}) \\
u'(t) &= (b-a)e^{-t} - bte^{-t} + o(e^{-t}) \\
u''(t) &= (-2b+a)e^{-t} + bte^{-t} + o(e^{-t}) \\
u'''(t) &= (3b-a)e^{-t} - bte^{-t} + o(e^{-t}).
\end{aligned}$$

Now suppose that for the even homoclinic orbit v which is our concern here, $b = 0$. Then

$$(v(t), v'(t), v''(t), v'''(t)) = (a, -a, a, -a)e^{-t} + o(e^{-t})$$

as $t \to \infty$. Now multiply the equation for v by $\phi(t) = e^t$ and integrate by parts over $(-\infty, x)$ to get, since $\phi = \phi' = \phi'' = \phi'''$,

$$\phi(x)[v''' - v'' + v' - v - 2v' + 2v](x) - \int_{-\infty}^{x} \phi(t) v^2(t) dt = 0.$$

Hence

$$\phi(x)(e^{-x}[-a - a - a - a + 2a + 2a] + o(e^{-x})) - \int_{-\infty}^{x} \phi(t) v^2(t) dt = 0.$$

Hence

$$0 = o(1) + \int_{-\infty}^{x} \phi(t) v^2(t) dt \text{ as } x \to \infty.$$

This is false. Hence $v(x) = bte^{-t} + ae^{-t} + o(e^{-t})$, as $t \to \infty$ and $b \neq 0$.

Thus the hypotheses required by (CHAMPNEYS & TOLAND, 1993) are verified and that theory applies to this equation.

3 A PLETHORA OF HOMOCLINIC ORBITS FOR $P \in (-2, 2)$

The purpose of this Section is to introduce basic notation, in particular a labelling of mulit-modal homoclinic orbits, which facilitates comparison of the Smale horseshoe dynamics (BELYAKOV & ŠIL'NIKOV, 1990), (DEVANEY, 1976), the more recent work on paths (CHAMPNEYS & TOLAND, 1993) and numerical experiments reported here for the first time. We begin by explaining the theory of paths (Section 3.1); then we give a brief discussion of numerical experiments (Section 3.2) which set the scene for a discussion of horseshoe dynamics (Section 3.3).

As observed in the Introduction, equation (1.1) may be expressed as a Hamiltonian system with two degrees of freedom.

$$\begin{cases} \dot{q} = Sp \\ \dot{p} = -\nabla V_\alpha(q) \end{cases} \tag{3.1}$$

where $\alpha = P + 2$, $S = \begin{pmatrix} 0 & 1 \\ 1 & 2 \end{pmatrix}$ and

$$V_\alpha(q) = -\frac{1}{2}(q_2 - \frac{1}{2}\alpha q_1)^2 + \frac{1}{2}q_1^2 - \frac{1}{3}q_1^3.$$

The Hamiltonian is given by $H(q,p) = \frac{1}{2}\langle Sp, p\rangle + V_\alpha(q)$.

When $P = -2$ ($\alpha = 0$), (3.1) has a unique homoclinic orbit which is the transverse intersection of the stable and unstable manifolds. After translation, the graph of this orbit, $\{u(t) : t \in \mathbb{R}\}$, is even about $t = 0$ and $u'(t) < 0$ for $t > 0$. Therefore, by continuity, there exists $\epsilon > 0$ such that, for $P \in (-2, -2+\epsilon)$, there is an even homoclinic orbit in the transverse intersection of the stable and unstable manifold whose graph, while uniformly close to that of the unique solution at $P = -2$, is no longer monotonic since 0 is a saddle-focus in this case. This orbit is what we referred to as the *primary* orbit in (CHAMPNEYS & TOLAND, 1993), $P \in (-2, -2+\epsilon)$, and as being uni-modal and symmetric.

3.1 Paths

Since S is indefinite, system (3.1) has a striking monotonicity property first introduced in (HOFER & TOLAND, 1984; TOLAND, 1986), which derives from the fact that, for any solution $(q(t), p(t))$ of (3.1) with zero Hamiltonian, $\langle S^{-1}\dot{q}(t), \dot{q}(t)\rangle$ is of constant sign as long as $V_\alpha(q(t)) \neq 0$. As S^{-1} is indefinite, the sets $\{q \in \mathbb{R}^2 : \langle S^{-1}q, q\rangle < 0\}$ and

$\{q \in \mathbb{R}^2 : \langle S^{-1}q, q\rangle > 0\}$ are open cones, each having exactly two components, respectively K_0, K_2 and K_1, K_3. Hence $\dot{q}(t) \in K_i$ for some fixed i as long as $V_\alpha(q(t)) \neq 0$. We notice that this monotonicity property concerns *paths* rather than orbits, the path of the orbit $\{(q(t), p(t)) : t \in \mathbb{R}\}$ being the set $\{q(t) : t \in \mathbb{R}\}$.

Briefly, we describe the behaviour, for t close to t_0, of paths of solutions with zero Hamiltonian if $V_\alpha(q(t_0)) = 0$ for some $t_0 \in \mathbb{R}$. Clearly $\langle S^{-1}\dot{q}(t_0), \dot{q}(t_0)\rangle = 0$ and therefore $\dot{q}(t)$ may switch from K_i to K_j $(j = i \pm 1 \bmod 4)$, when t crosses the value t_0. This is exactly what happens when $\langle \nabla V_\alpha(q(t_0)), \dot{q}(t_0)\rangle \neq 0$, because then $\sigma = (\mathrm{d}/\mathrm{d}t)V_\alpha(q(t_0)) \neq 0$ and the sign of $V_\alpha(q(t))$ changes at $t = t_0$; moreover K_i and K_j are related by $\dot{q}(t_0) \in \partial K_i \cap \partial K_j$, and the future behaviour of $q(t)$ (for $t > t_0$) will depend only on which ray of ∂K_i the vector $\dot{q}(t_0)$ belongs to (∂K_i being the union of two rays) and the sign of σ.

The cases when $\dot{q}(t_0) \neq 0$ and $\langle \nabla V_\alpha(q(t_0)), \dot{q}(t_0)\rangle = 0$ or when $\dot{q}(t_0) = 0$, which are more difficult, are discussed in (AMICK & TOLAND, 1991) and (CHAMPNEYS & TOLAND, 1993). When $\langle \nabla V_\alpha q(t_0), \dot{q}(t_0)\rangle = 0$ it is shown that (i) if $\{\nabla V_\alpha(q(t_0))\}^\perp \subset K_0 \cup K_2$, then $\dot{q}(t_0) = 0$ and $V_\alpha(q(t)) < 0$ for $|t - t_0| > 0$ small; (ii) if $\{\nabla V_\alpha(q(t_0))\}^\perp \subset K_1 \cup K_3$, then $\dot{q}(t_0) = 0$ and $V_\alpha(q(t)) > 0$ for $|t - t_0| > 0$ small, and, finally, (iii) if $\{\nabla V_\alpha(q(t_0))\}^\perp \subset \{q \in \mathbb{R}^2 | \langle S^{-1}q, q\rangle = 0\}$ and if the curve $\{q \in \mathbb{R}^2 | V_\alpha(q) = 0\}$ has non-null curvature at $q(t_0)$, then $q(t)$ remains on the concave side for $|t - t_0| > 0$ small. Cases (i) and (ii) correspond to points of symmetry of the path.

Recall, from the Introduction, the nature of the equilibrium at 0 for various values of P. It has been noted in (CHAMPNEYS & TOLAND, 1993) that the nature of this equilibrium may also be determined geometrically from the relative positions of the sets $\{x \in \mathbb{R}^2 | \langle S^{-1}x, x\rangle = 0\}$ and $\{x \in \mathbb{R}^2 | \langle V_\alpha''(0)x, x\rangle = 0\}$. Note that $V_\alpha''(0)$ is an invertible indefinite matrix, and therefore $\{x \in \mathbb{R}^2 | \langle V_\alpha''(0)x, x\rangle = 0\}$ is the union of two straight lines intersecting each other at 0. If $P < -2$, $\{x \in \mathbb{R}^2 | \langle V_\alpha''(0)x, x\rangle \geq 0\} \subset \{x \in \mathbb{R}^2 | \langle S^{-1}x, x\rangle < 0\}$, if $P \in (-2, 2)$, $\langle S^{-1}x, x\rangle$ takes both signs on $\{x \in \mathbb{R}^2 | \langle V_\alpha''(0)x, x\rangle > 0\}$, and $\{x \in \mathbb{R}^2 | \langle V_\alpha''(0)x, x\rangle \geq 0\} \subset \{x \in \mathbb{R}^2 | \langle S^{-1}x, x\rangle > 0\}$ if $P > -2$. (In the degenerate cases $P = \pm 2$ there are at most three distinct lines of zeros of the two quadratic forms.)

The case of interest here is $P \in (-2, 2)$, i.e. $0 < \alpha < 4$, and Figure 3 illustrates the zero level sets of $V_\alpha(q)$ and $\langle S^{-1}q, q\rangle$, $q \in \mathbb{R}^2$, for some $\alpha \in (0, 2)$. First note the set $\{q \neq 0 : V_\alpha(q) = 0\}$ has four components near 0, denoted by Σ_i $(0 \leq i \leq 3)$, each being tangent at 0 to one of the two lines in $\{x \in \mathbb{R}^2 | \langle V_\alpha''(0)x, x\rangle = 0\}$. Moreover, we choose

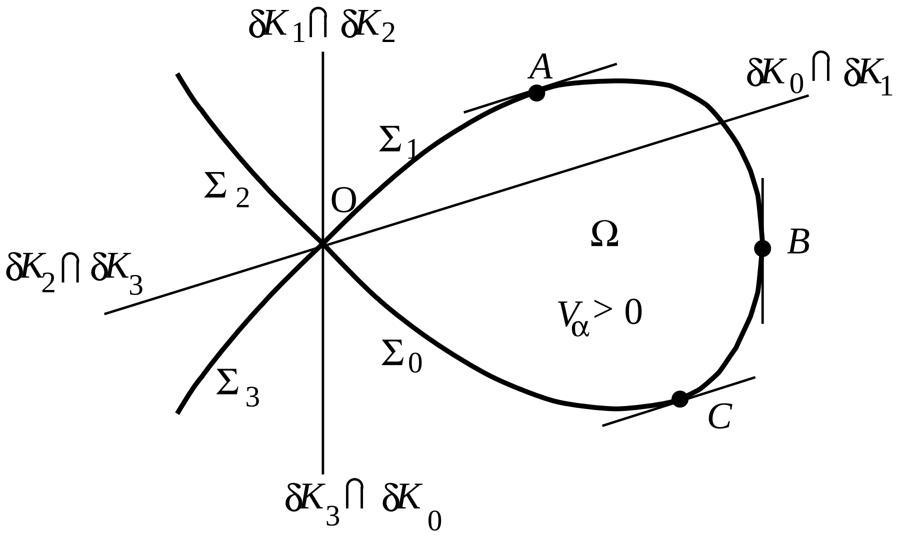

Figure 3: *The geometrical configuration. See text for explanation.*

labels as in Figure 3, where $\langle S^{-1}x, x\rangle$ is negative on Σ_0 and V_α is positive on $\partial K_0 \cap \partial K_1$ in a neighbourhood of 0.

If the path $\{q(t), t \text{ sufficiently large}\}$, of a solution of (3.1), remains in an explicit neighbourhood of $0 \in \mathbb{R}^2$ (namely the neighbourhood $\mathcal{N}$ introduced below) and $\dot{q}(t) \in \partial K_{i+1} \cap \partial K_{i+2}$ when $q(t) \in \Sigma_i$, then $q(t)$ rotates anticlockwise around 0 and even tends exponentially to zero if $P \in (-2, 0)$ as illustrated in Figure 4(a) (see (BUFFONI, 1993a; BUFFONI & TOLAND, n.d.; CHAMPNEYS & TOLAND, 1993)). If $q(t_0) \in \Sigma_i$ and $\dot{q}(t_0) = 0$, then $q(t)$ will belong to the region between Σ_{i-1} and Σ_i for small $|t - t_0| > 0$; see Figure 4(b). If $q(t_0) \in \Sigma_i$ and $\dot{q}(t_0) \in \partial K_i \cap \partial K_{i+1}$, then $q(t)$ may begin to go away from 0 and even to rotate clockwise around 0 (Figure 4(c)). Geometrical considerations like these are crucial to the multiplicity results of (BUFFONI, 1993a; BUFFONI & TOLAND, n.d.; CHAMPNEYS & TOLAND, 1993).

Another basic ingredient of the analysis is the behaviour of paths outside $\mathcal{N}$. For $P \in (-2, 2)$, the sets $\{x : V_\alpha(x) = 0\}$ and $\{x | \langle S^{-1}x, x\rangle = 0\}$ are depicted in Figure 3 in a neighbourhood of 0. The set $\{q \in \mathbb{R}^2 | \, V_\alpha(q) > 0\}$ has a bounded convex component Ω and $\partial\Omega$ is divided into three parts by the points $0, A, B, C$ in $\partial\Omega$ defined by $\{\nabla V_\alpha(x)\}^\perp \subset \{q \in \mathbb{R}^2 | \langle S^{-1}q, q\rangle = 0\}$ for $x = A, B, C$ and enumerated in clockwise order. This has an obvious geometrical interpretation: at A and C the tangent to $\mathcal{C}$ is parallel to $\partial K_0 \cap \partial K_1$ and at B it is parallel to $\partial K_1 \cap \partial K_2$ (see Figure 3). If $\dot{q}(t_0) = 0$ and $q(t_0) \in \partial\Omega$, then $q(t)$ is either in Ω or outside $\bar{\Omega}$ for $t > t_0$ near t_0 according to Figure 5 (see (AMICK

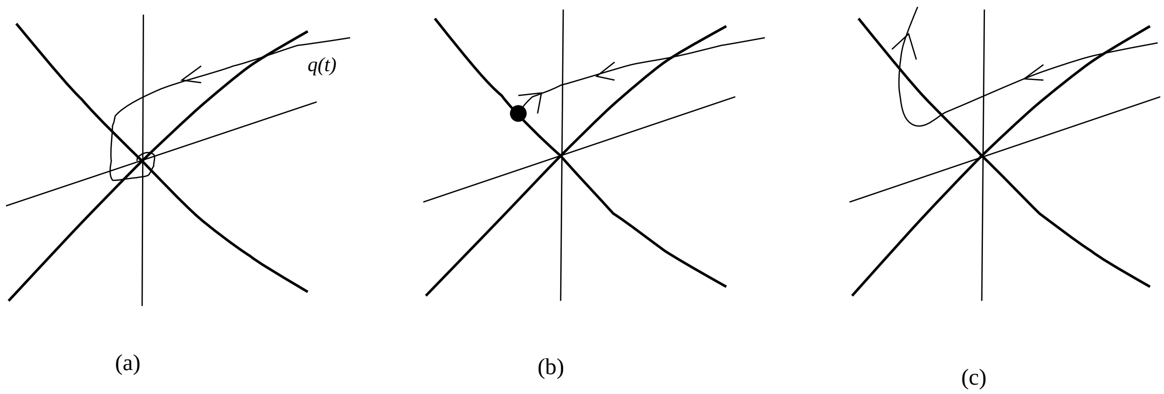

Figure 4: *The behaviour of paths as a consequence of the geometry near the origin. See text for explanation.*

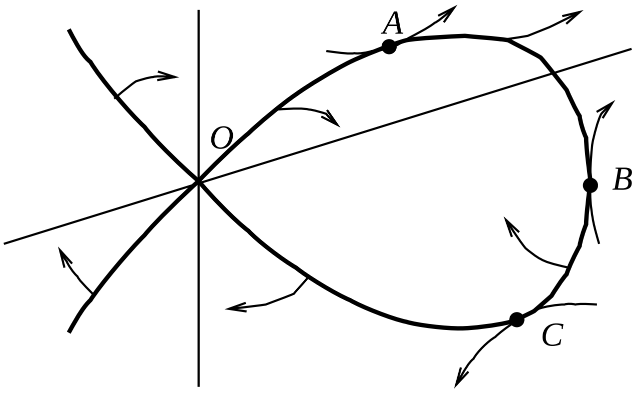

Figure 5: *The behaviour of paths at symmetric points*

& TOLAND, 1991; CHAMPNEYS & TOLAND, 1993; TOLAND, 1986)).

For t near $-\infty$, the path of any one of the homoclinic orbits found in (CHAMPNEYS & TOLAND, 1993) and (BUFFONI, 1993a) lies in a convex neighbourhood $\mathcal{N}$ of 0 which does not intersect $\{A, B, C\}$. As t increases the path rotates clockwise about 0 until, at some time when it enters Ω at a point of OA, it passes monotonically across Ω to a point of BC, where it leaves Ω only to return again to Ω, crossing $\partial\Omega$ again between B and C. Subsequently it passes across Ω, and meets $\partial\Omega$ next at a point in $\mathcal{N}$. This process may be repeated many times before the orbits in question finally converge to 0. An orbit is called *n-modal* if its path leaves $\mathcal{N}$ exactly n times as t increases from $-\infty$ to ∞. The notation $\mathbf{n}(\ell_1, \ldots, \ell_{n-1})$ is used for an n-modal homoclinic solution ($n \geq 2$) whose path intersects $\{V_\alpha = 0\}$ exactly $2\ell_k$ times during its kth return to $\mathcal{N}$ (if q crosses $\{V_\alpha = 0\}$ at 0 or meets it with zero velocity (which cannot both occur simultaneously), then we count this intersection twice). The homoclinic solutions found in (CHAMPNEYS & TOLAND, 1993) are of the form $\mathbf{2}(\ell)$, $\ell \geq 1$, and those found in (BUFFONI, 1993a) of the form $\mathbf{n}(1,\ldots,1)$ for $n \geq 1$. In the first case the homoclinic orbits were shown to exist for all $P \in (-2, -2+\epsilon)$ (ϵ small) and in the second case for all $P \in (-2, 0]$.

In fact, the numerical results which follow suggest that a homoclinic solution of the form $\mathbf{n}(\ell_1, \ldots, \ell_{n-1})$ exists for all $n \geq 2$, $\ell_1, \ldots, \ell_{n-1} \geq 1$ and all $P \in (-2\,, 1.5]$.

3.2 Numerical considerations

Before considering the horseshoe dynamics in the next Subsection, we pause to consolidate the theory of paths by illustrating it with some numerical experiments. At the same time we take the opportunity to explain how the graphs of solutions u of (1.1) can be used in the presentation and interpretation of results on the phase plane of (3.1) in $\mathbb{R}^4$.

The following observations are made with reference to Figures 3, 6 and 7. Note that in the original variables of (1.1),

$$V_\alpha(q) = W(u, u'') = \frac{1}{2}u''^2 - \frac{1}{2}u^2 + \frac{1}{3}u^3, \tag{3.2}$$

so that, in the co-ordinates (u, u''), W and its zero level set are independent of P (the zero level-set of V_α is represented in these co-ordinates in Figures 2 — 5 above). Hence, at least for P close to -2, we can make the following interpretations of the intersection of a path $q(t)$ with $\{V = 0\}$ within $\mathcal{N}$:

$$\begin{aligned} q(t) \in \Sigma_1 \quad &\Rightarrow \quad u > 0,\ u'' > 0; \\ q(t) \in \Sigma_2 \quad &\Rightarrow \quad u < 0,\ u'' > 0; \\ q(t) \in \Sigma_3 \quad &\Rightarrow \quad u < 0,\ u'' < 0; \\ q(t) \in \Sigma_0 \quad &\Rightarrow \quad u > 0,\ u'' < 0. \end{aligned}$$

This is reflected in the numerical observation that the $2\ell_k$ intersections with $\{W = 0\}$ during the kth return to $\mathcal{N}$ of the path of an orbit with symbol $\mathbf{n}(\ell_1, \ldots, \ell_{n-1})$ correspond to $[\ell_k/2]$ oscillations in the graph of the orbit. Here $[\ \cdot\ ]$ denotes the integer part of a real number. More precisely there are $2[l_k/2]$ crossings of the u-axis and $2[(\ell_k - 1)/2] + 1$ local extrema between adjacent humps which are local maxima. Moreover, during each intervening time spent outside $\mathcal{N}$ there is a large "hump" in the graph. Hence the graph of the primary orbit has a single hump, a bi-modal orbit $\mathbf{2}(\ell)$ has two humps separated

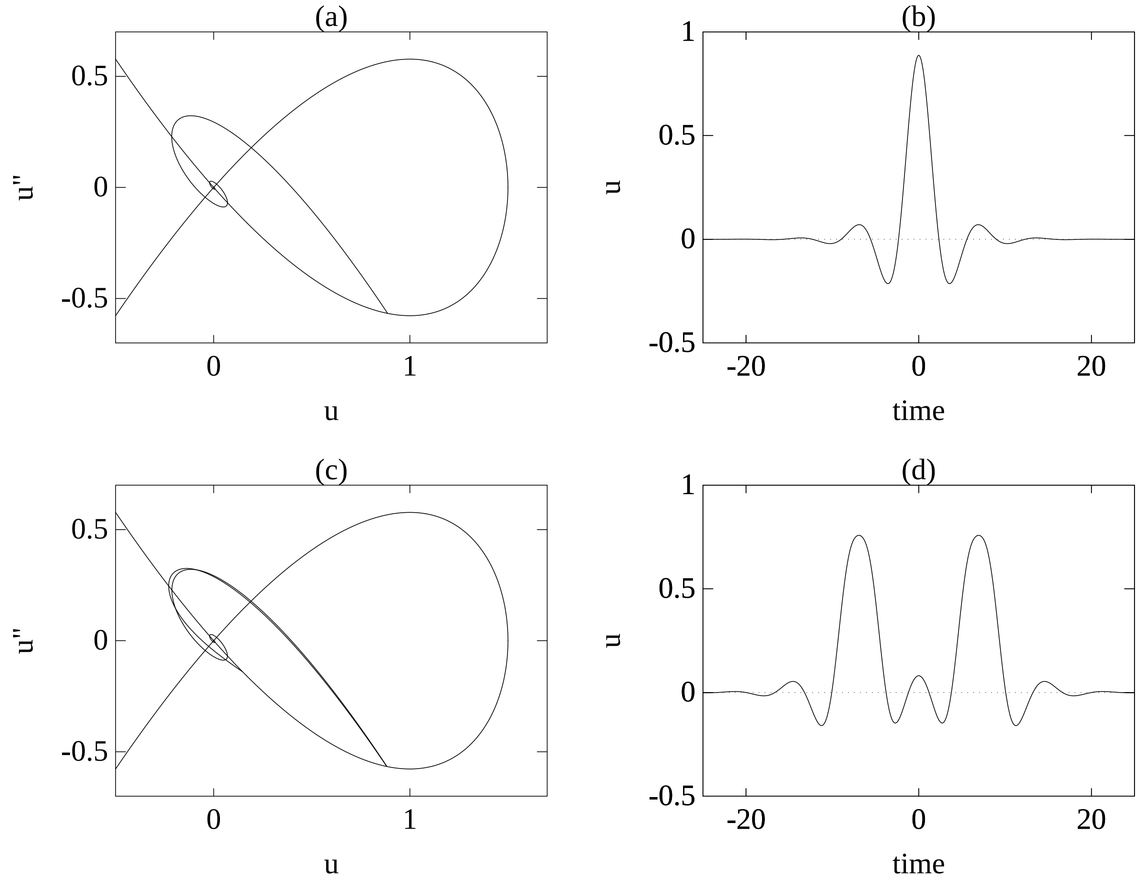

Figure 6: *Illustrating the correspondence between paths and graphs for numerically calculated orbits with* $P = 1.5$. *(a) and (b) depict the path and graph, respectively, of the primary orbit; (c) and (d) depict the bi-modal orbit* $\mathbf{2}(4)$.

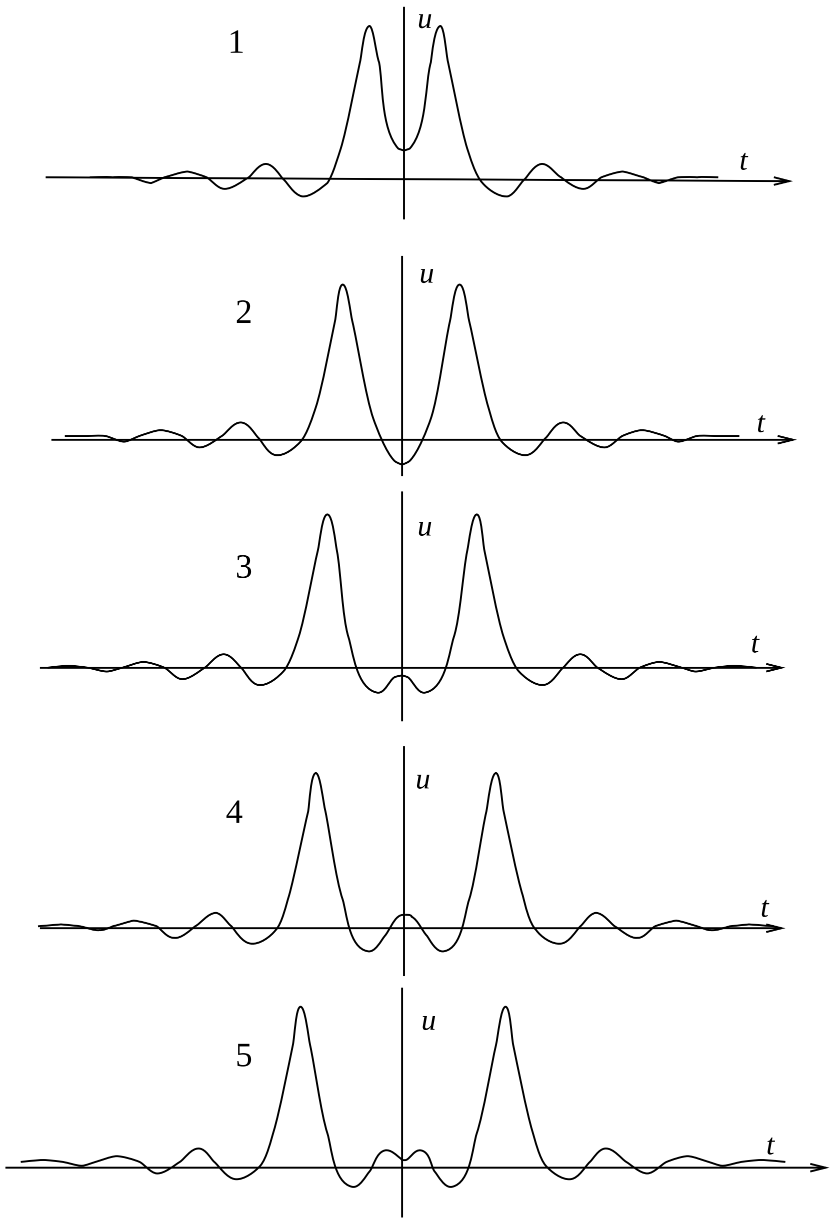

Figure 7: *Schematic diagram illustrating the portions of graphs corresponding to symbols 1–5, specifically represented are the bi-modal orbits* $\mathbf{2}(k)$ *for* $k = 1, \ldots 5$.

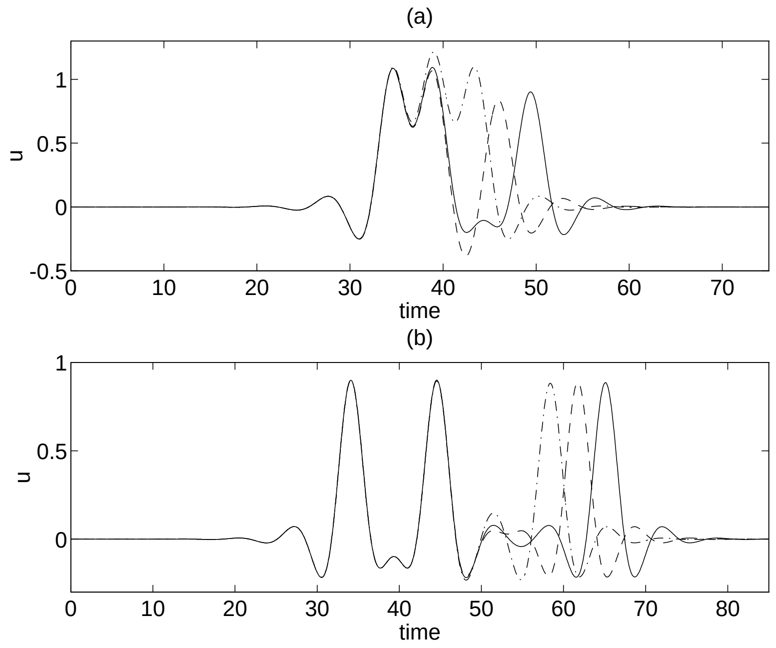

Figure 8: *Graphs of tri-modal orbits at* $P = 1.5$*. (a)* $\mathbf{3}(1, j)$*, for* $j = 1, 2, 3$*; (b)* $\mathbf{3}(3, j)$*, for* $j = 4, 5, 6$*. For* $t < 30$ *the graphs are indistinguishable.*

by $[\ell/2]$ oscillations, a tri-modal orbit $\mathbf{3}(\ell_1, \ell_2)$ has three humps which are separated by $[\ell_1/2]$ and $[\ell_2/2]$ oscillations, etc. Finally, the infinite number of exponentially decaying rotations about the origin of the path of an orbit tending to 0 (as depicted in Figure 6(a)) correspond to the existence of infinitely many decaying oscillations in the two "tails" of the graph of a homoclinic orbit.

Note that it is theoretically possible to read off the label of a homoclinic orbit from its graph, in the manner just described, only for P near -2. For much larger P, it is impossible to distinguish between oscillations, humps and the tail of the graph because, for example, paths may leave $\mathcal{N}$ outside Ω or cross the origin in q-space (this lack of distinction is fundamental to the coalescence results described in Sections 4-6 below). Hence, the only way a homoclinic orbit can reliably be labelled in numerical experiments is to follow the branch of solutions on which the orbit lies, *obtained by decreasing* P, and to assign a label according to the type of solution into which it evolves as $P \to -2$. In other words, branches of solutions, rather than individual orbits must be labelled. Nevertheless we have found, somewhat surprisingly, that, in practice, $P = 1.5$ seems to be an adequately small P-value at which to assign labels to homoclinic orbits.

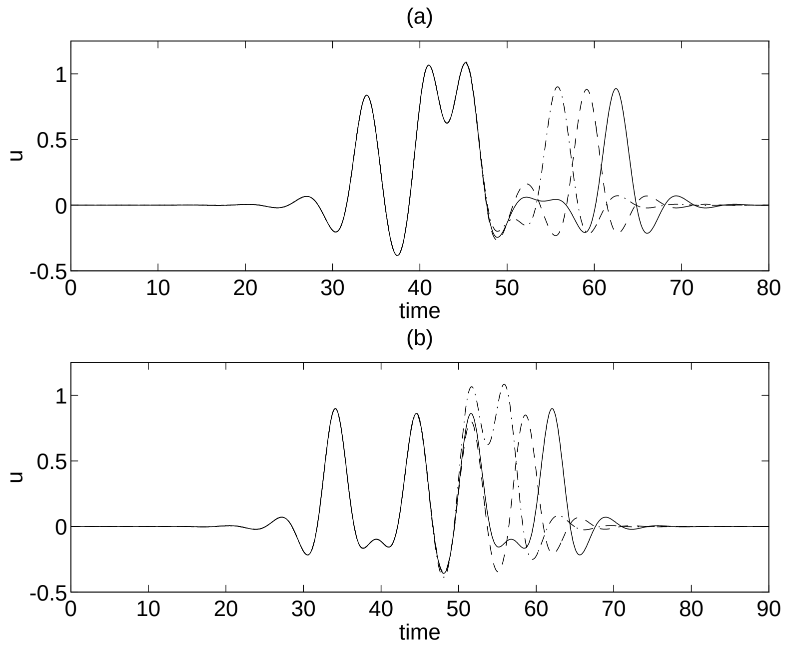

Figure 9: *Graphs of 4-modal orbits at* $P = 1.5$*. (a)* $\mathbf{4}(2,1,j)$*, for* $j = 3,4,5$*; (b)* $\mathbf{4}(3,2,j)$*, for* $j = 1,2,3$*. For* $t < 30$ *the graphs are indistinguishable.*

Henceforth we will use graphs to depict orbits whose profiles have been obtained numerically. Numerical computations of symmetric homoclinic orbits presented elsewhere ((CHAMPNEYS, 1994; CHAMPNEYS & SPENCE, 1993; CHAMPNEYS & TOLAND, 1993)) suggest that homoclinic orbits with every symmetric label $\mathbf{n}(\ell_1,\ldots,\ell_{n-1})$, $\ell_1,\ldots,\ell_{n-1} \geq 1$ with $\ell_i = \ell_j$ for $i+j = n$, exist at the fixed value $P = 1.5$. Moreover, branches of each of the computed orbits were followed numerically by decreasing P; although there are numerical dificulties with computing multi-modal orbits near $P = -2$ (see (CHAMPNEYS & SPENCE, 1993)) the results were consistent with each orbit existing for all $P \in (-2, 1.5]$. Those results were all obtained using symmetric-section boundary conditions, which precludes the possibility of finding asymmetric homoclinic orbits. Here we present orbits calculated numerically using full asymptotic boundary conditions. Figures 8 and 9 depict certain tri-modal and four-modal homoclinic orbits obtained using shooting at $P = 1.5$. Observe that those orbits labelled by a symmetric symbol sequence are themselves symmetric (e.g. $\mathbf{3}$(1,1) and $\mathbf{4}$(3,2,3)). Note also that the graphs of orbits $\mathbf{4}$(2,2,3) and $\mathbf{4}$(3,2,2), whose symbol sequences are reversals of one another, are images of each other under the symmetry $t \to -t$.

We have computed many more asymmetric homoclinic orbits than are presented in Figures 8 and 9. The numerical method is less stable than that using symmetric-section boundary conditions and requires computation over longer time intervals, in practice making it hard to compute n-modal asymmetric homoclinic orbits for $n \geq 5$. Nevertheless, there is, so far, no numerical evidence for any symbol sequence of the form $\mathbf{n}(\ell_1, \ldots, \ell_{n-1})$, $n \geq 2$, $\ell \geq 1$ for which there is not a corresponding homoclinic orbit at $P = 1.5$. We have also followed loci of many asymmetric orbits with decreasing P. In each case, the results are consistent with the branches existing for all $P \in (-2, 1.5]$.

3.3 Horseshoe dynamics

As this Hamiltonian system has two degrees of freedom and a non-degenerate primary homoclinic orbit γ_α to the saddle-focus equilibrium 0, for all $P = \alpha - 2 \in (-2, -2 + \epsilon)$, $\epsilon > 0$), Devaney's construction (DEVANEY, 1976) of symbolic dynamics (i.e. Smale horseshoes) can be applied. As stated in (BELYAKOV & ŠIL'NIKOV, 1990) it follows that there exist infinitely many homoclinic orbits. Specifically, for some small neighbourhood of γ_α (γ_α and this neighbourhood depending upon P), the set of all orbits homoclinic to 0 lying entirely in this small neighbourhood is countable and in *one-to-one correspondence* (excepting γ_α) with the set of finite "segments" (so called in (BELYAKOV & ŠIL'NIKOV, 1990))

$$\{[j_1, \ldots, j_k] \ \ |k, j_1, \ldots, j_k \in \mathbb{Z}^+\}. \tag{3.3}$$

We now give a short description of the construction of this family of homoclinic orbits. We restrict attention to nonlineasr Hamiltonian systems which have a non-degenerate primary homoclinic orbit and which are linear in a neighbourhood of the origin. We refer the reader to (WIGGINS, 1988) for a discussion of the general case.

Consider the Hamiltonian system

$$J\dot{x} = \nabla H(x) \quad , \quad x \in \mathbb{R}^4,$$

where $J = \begin{pmatrix} 0 & I \\ -I & 0 \end{pmatrix}$, $H : \mathbb{R}^4 \to \mathbb{R}$ is smooth, quadratic in a neighbourhood of the origin, $A = H''(0)$ is non-singular and the eigenvalues of $J^{-1}A$ are $\pm\lambda \pm i\omega$, $\lambda < 0, \omega > 0$. We suppose that the system admits a homoclinic orbit to 0, denoted by γ, on which the stable and unstable manifolds intersect transversally.

After a symplectic linear transformation, we may suppose that

$$J^{-1}A = \begin{bmatrix} \lambda & -\omega & 0 & 0 \\ \omega & \lambda & 0 & 0 \\ 0 & 0 & -\lambda & -\omega \\ 0 & 0 & \omega & -\lambda \end{bmatrix}.$$

Let $h > 0$ be small enough and set

$$B = \{x \in \mathbb{R}^4 \mid x_1^2 + x_2^2 \leq h, \quad x_3^2 + x_4^2 \leq h\}.$$

The local stable and unstable manifold are given by

$$W^s_{\mathrm{loc}} = \{x \in B \mid x_3 = x_4 = 0\}$$

and

$$W^u_{\mathrm{loc}} = \{x \in B \mid x_1 = x_2 = 0\}$$

(for h sufficiently small). We introduce the new coordinates

$$\begin{cases} x_1 = r_1 \cos\theta_1 \\ x_2 = r_1 \sin\theta_1 \end{cases}, \quad \begin{cases} x_3 = r_2 \cos\theta_2 \\ x_4 = r_2 \sin\theta_2 \end{cases}.$$

Note that

$$A = \begin{pmatrix} 0 & 0 & \lambda & \omega \\ 0 & 0 & -\omega & \lambda \\ \lambda & -\omega & 0 & 0 \\ \omega & \lambda & 0 & 0 \end{pmatrix},$$

and, for $|x|$ small, $H(x) = 0$ if, and only if, $r_1 r_2 = 0$ or $\theta_2 - \theta_1 = \alpha \bmod \pi$, where α is a constant depending upon λ and ω. Define T_1 and T_2 by

$$\begin{aligned} T_1 &= \{x \in B | r_1 = h \ , \ 0 \leq r_2 < h\} \subset B, \\ T_2 &= \{x \in B | r_2 = h \ , \ 0 \leq r_1 < h\} \subset B \ . \end{aligned}$$

These sets are homeomorphic to the interiors of two tori with $W^s_{\mathrm{loc}} \cap T_1$ and $W^u_{\mathrm{loc}} \cap T_2$ corresponding to their central circles, (see Figure 10). Moreover, the set $T_1 \cap \{H = 0\}$ is homeomorphic to a two-dimensional cylinder containing the circle $W^s_{\mathrm{loc}} \cap T_1$ (see Figure 11). The same holds for $T_2 \cap \{H = 0\} \supset W^u_{\mathrm{loc}} \cap T_2$. The equation of the flow near 0 is given by

$$\dot{r}_1 = \lambda r_1 \ , \ \dot{\theta}_1 = \omega \ , \ \dot{r}_2 = -\lambda r_2 \ , \ \dot{\theta}_2 = \omega.$$

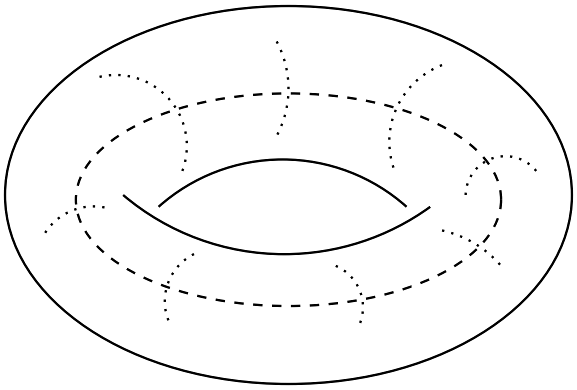

Figure 10: T_1 *with* $W^s_{\rm loc} \cap T_1$ *inside (dashed circle).*

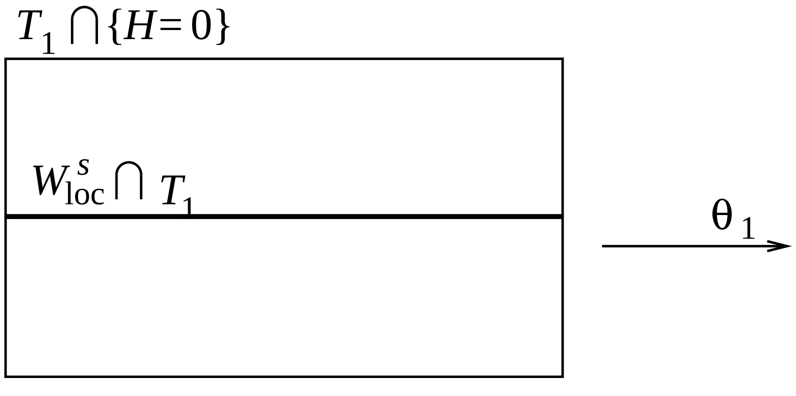

Figure 11: *The left and right sides are identified in order to obtain a cylinder.*

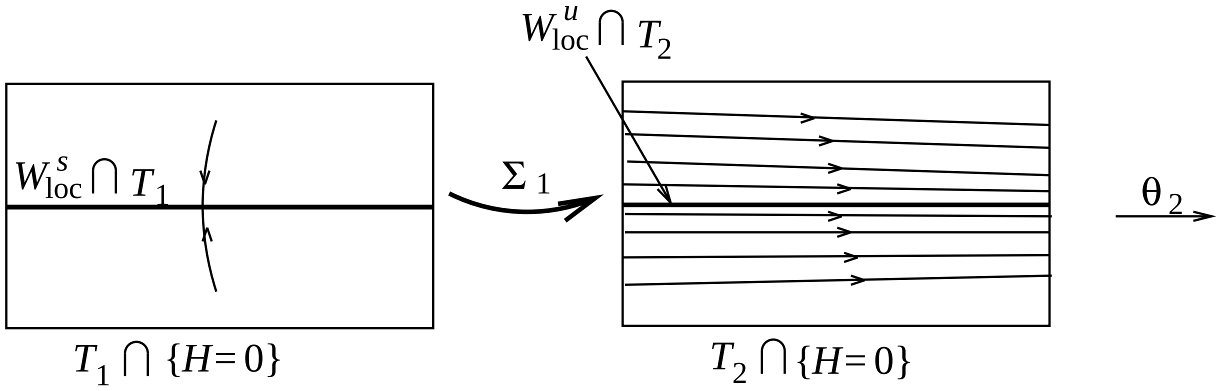

Figure 12: *The left and right sides of each rectangle are identified to obtain cylinders.*

Let Σ_1 be the Poincaré map given by the flow near the origin which sends $x^{(1)} \in T_1 - W^s_{\rm loc}$ to $x^{(2)} \in T_2 - W^u_{\rm loc}$ with

$$r_1^{(2)} = r_2^{(1)} \ , \ \theta_1^{(2)} = \theta_1^{(1)} - \frac{\omega}{\lambda} \log\left(\frac{h}{r_2^{(1)}}\right) ,$$

$$r_2^{(2)} = h \ , \ \theta_2^{(2)} = \theta_2^{(1)} - \frac{\omega}{\lambda} \log\left(\frac{h}{r_2^{(1)}}\right) \ .$$

The time needed is given by $-\lambda^{-1}\log(h/r_2^{(1)})$. From this formula, it is clear that the image of a curve in $T_1 \cap \{H = 0\}$ which intersects $W^s_{\rm loc} \cap T_1$ transversally is the union of two curves in $T_2 \cap \{H = 0\}$ which spiral toward $W^u_{\rm loc} \cap T_2$, (see Figure 12).

Considering the flow in a neighbourhood of the homoclinic orbit γ, we obtain a one-to-one Poincaré map Σ_2 from a neighbourhood Π_2 in $T_2 \cap \{H = 0\}$ of $\gamma \cap T_2$ to a neighbourhood Π_1 in $T_1 \cap \{H = 0\}$ of $\gamma \cap T_1$. This is the situation depicted in Figure 13. The global stable manifold is defined by

$$W^s_{\rm gl} = \Sigma_2^{-1}(W^s_{\rm loc} \cap \Pi_1) \subset \Pi_2.$$

By assumption $W^s_{\rm gl}$ intersects $W^u_{\rm loc} \cap \Pi_2$ transversally.

The set $\Sigma_1^{-1}(W^s_{\rm gl})$ intersects Π_1 at a family of "horizontal" curves, each being inside a "horizontal" strip S_k with $\cup_{k\geq 1} S_k = \Sigma_1^{-1}(\Pi_2) \cap \Pi_1$. Devaney (DEVANEY, 1976), (see Wiggins (WIGGINS, 1988)) shows that the time needed by Σ_1 to send the strip S_k to Π_2 is approximately equal to

$$C + k\frac{\pi}{w} \tag{3.4}$$

where $C > 0$ is constant.

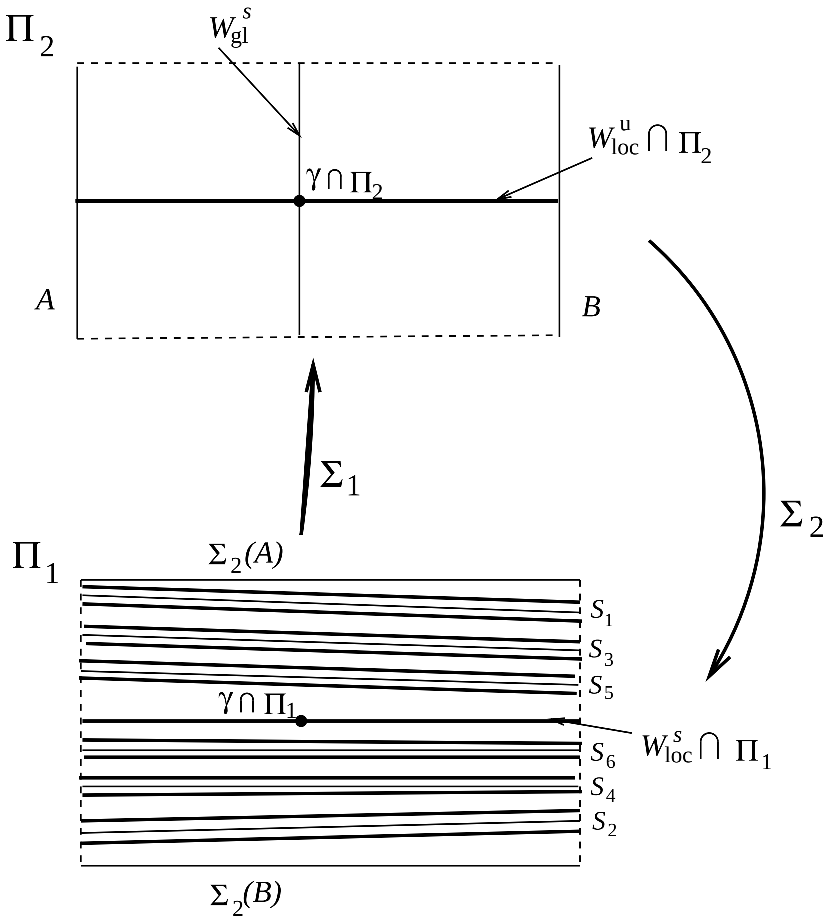

Figure 13: *In this figure, lines depicted as straight represent curves. The curves in the strips S_k are pieces of $\Sigma_1^{-1}(W^s_{g\ell})$.*

Put an orientation on $W^u_{\text{loc}} \cap \Pi_2$ (for example from the "side" A to the "side" B, i.e. θ_2 is increasing). Then $\Sigma_2(W^u_{\text{loc}} \cap \Pi_2)$ is a curve going from $\Sigma_2(A)$ to $\Sigma_2(B)$ intersecting each strip S_k transversally. Denote by $[W^u_{\text{loc}}]_k \subset W^u_{\text{loc}} \cap \Pi_2$ the segment that corresponds to S_k. Note that we may suppose the S_k with k odd (respectively even) to lie between $W^s_{\text{loc}} \cap \Pi_1$ and $\Sigma_2(A)$ (respectively $\Sigma_2(B)$). The $[W^u_{\text{loc}}]_k$ are disjoint and $(\Sigma_1 \circ \Sigma_2)([W^u_{\text{loc}}]_k)$ is a curve intersecting W^s_{gl} transversally from A to B if k is odd (same orientation as $W^u_{\text{loc}} \cap \Pi_2$) and from B to A if k is even (opposite orientation). Each such intersection gives the existence of a bi-modal homoclinic orbit. Moreover each $[W^u_{\text{loc}}]_k$ contains a point of a bimodal homoclinic orbit and we label that orbit $[k]$. These bimodal homoclinic orbits are ordered on $W^u_{\text{loc}} \cap \Pi_2$ as follows:

$$[1], [3], [5], \ldots, [k], \ldots, [6], [4], [2].$$

Taking $(\Sigma_1 \circ \Sigma_2)([W^u_{\text{loc}}]_k)$ instead of $W^u_{\text{loc}} \cap \Pi_2$, we obtain $[W^u_{\text{loc}}]_{k\ell} \subset [W^u_{\text{loc}}]_k$ such that $\Sigma_2 \circ \Sigma_1 \circ \Sigma_2([W^u_{\text{loc}}])$ is a curve crossing the strip S_ℓ.

The $[W^u_{\text{loc}}]_{k\ell}$ are disjoint and each contains a point of a trimodal homoclinic orbit, which we label by $[k, \ell]$. They are ordered in $[W^u_{\text{loc}}]_k$ in the following way:

$$[k,1], [k,3], [k,5], \ldots, [k], \ldots, [k,6][k,4], [k,2] \text{ if } k \text{ is odd },$$

$$[k,2], [k,4], [k,6], \ldots, [k], \ldots [k,5], [k,3], [k,1] \text{ if } k \text{ is even}.$$

By iteration, we obtain the whole family of homoclinic solutions given by (3.3) with a specific ordering. This ordering is interpreted in the present setting in Definition 3.1 below.

Inspecting the above description, we first observe that the orbit $[j_1, \ldots, j_k]$ corresponds to a homoclinic orbit which visits a small neighbourhood of $0 \in \mathbb{R}^4$ exactly k times (not counting the infinite time-intervals spent in this neighbourhood as $t \to \pm\infty$, the i^{th} visit of duration approximately proportional to j_i. In fact, if t_i is the duration of the i^{th} visit then (3.4) suggests that $t_i/j_i \to \pi/\omega$ as $j_i \to \infty$, and j_i counts the approximate number of half-turns about the origin a trajectory makes close to the stable and unstable manifolds during the i^{th} visit to the small neighbourhood of 0 in $\mathbb{R}^4$. Thus we may conjecture that such a homoclinic orbit $[j_1, \ldots, j_{n-1}]$, $n \geq 2$, is the one found numerically and previously labelled by $\mathbf{n}(s + j_1, \ldots, s + j_{n-1})$ for some integer s. Here s may depend upon $P \in (-2, -2 + \epsilon)$, and it is not clear if $s = 0$ *a priori*. Whether or not this is so depends on the size of C

in (3.4). The number s arises, in principle, as follows. In the construction of the Smale horseshoe, it was essential to carry out the analysis on a Poincaré section Π_1 transverse to γ_α, where Π_1 is required to be sufficiently close to 0 for various estimates to hold. Since the path of γ_α encircles the origin in an anticlockwise sense infinitely often as $t \to \infty$, it is to be expected that Π_1 lies so close to 0 that the path has already encircled the origin and met $\{W = 0\}$ many times before reaching Π_1, (W is defined in (3.2)). The elements j_i of the segment $[j_1, \ldots, j_{n-1}]$ only count the number of times an orbit winds around 0 between intersections with Π_1 and Π_2. To these must be added the number of winds in $\mathcal{N}$ which preceded its first arrival at Π_1 and which followed its next pass through a neighbourhood of Π_2. Thus we add an integer, s say, to j_i. However, we conjecture, based on numerical results, that for all $P \in (-2, -2+\epsilon)$, this neighbourhood of γ_0 may be chosen such that $s = 0$ (i.e. no extra winds). Finally, we interpret the ordering of homoclinic orbits labelled $[j_1, \ldots, j_{n-1}]$, in the present setting, as saying that for all $P \in (-2, -2+\epsilon)$, homoclinic orbits corresponding to all possible labels $\mathbf{n}(\ell_1, \ldots, \ell_{n-1}), n \geq 2, \ell_1, \ldots, \ell_{n-1} \geq 1$, exist and are ordered in the local unstable manifold in the following way. First, and for the purposes of this definition only, add the symbol ∞ at the end of each $\mathbf{n}(\ell_1, \ldots, \ell_{n-1})$, i.e. set $\ell_n = \infty$, and denote the primary orbit by $\mathbf{1}(\infty)$; second, introduce the following total ordering on $\mathbb{N} \cup \{\infty\}$:

$$1 \prec 3 \prec 5 \prec 7 \prec \ldots \prec \infty \prec \ldots \prec 8 \prec 6 \prec 4 \prec 2;$$

finally, extend this total ordering to homoclinic orbits as follows.

Definition 3.1 *Consider two distinct sequences* $\mathbf{n}(\ell_1, \ldots, \ell_n)$ *and* $\bar{\mathbf{n}}(\bar{\ell}_1, \ldots, \bar{\ell}_{\bar{n}})$ *with* $\ell_n = \bar{\ell}_{\bar{n}} = \infty$. *Let* $k \in \{1, \ldots, \min(n, \bar{n})\}$ *be the smallest index at which these two sequences differ. Then write*

$$\mathbf{n}(\ell_1, \ldots, \ell_n) \prec \bar{\mathbf{n}}(\bar{\ell}_1, \ldots, \bar{\ell}_{\bar{n}})$$

if and only if either

$$\ell_k \prec \bar{\ell}_k \quad \textit{and} \quad \textit{card}\{i : \ell_i \in 2\mathbb{Z} | 1 \leq i \leq k-1\} \in 2\mathbb{Z}$$

or

$$\bar{\ell}_k \prec \ell_k \quad \textit{and} \quad \textit{card}\{i : \ell_i \in 2\mathbb{Z} | 1 \leq i \leq k-1\} + 1 \in 2\mathbb{Z}.$$

For example

$$\mathbf{3}(1,1) \prec \mathbf{2}(1) \prec \mathbf{3}(1,2) \prec \mathbf{3}(3,1) \prec \mathbf{2}(3) \prec \mathbf{3}(3,2) \prec \mathbf{1}(\infty)$$

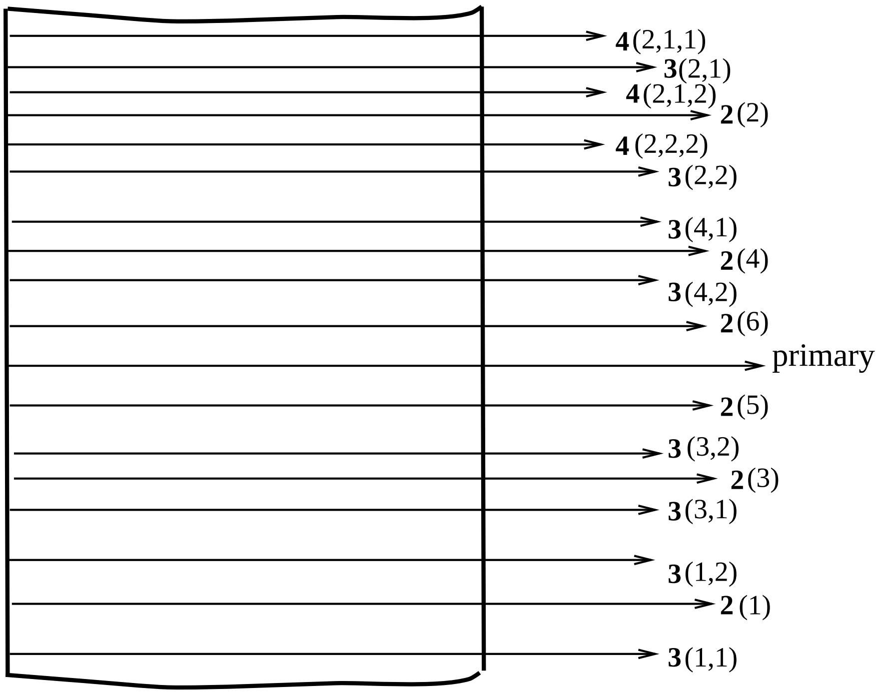

Figure 14: *The numerically observed ordering of certain homoclinic orbits, which can be seen to agree with Definition* 3.1

$$\prec \mathbf{3}(4,2) \prec \mathbf{2}(4) \prec \mathbf{3}(4,1) \prec \mathbf{3}(2,2) \prec \mathbf{2}(2) \prec \mathbf{3}(2,1).$$

Note that all bimodal orbits with an even number of oscillations are on one side of the primary homoclinic orbit and all bimodals with an odd number are on the other side. If we now focus attention on the local unstable manifold near a bimodal orbit of type $\mathbf{2}(\ell-1)$ we also have that the tri-modal orbits $\mathbf{3}(\ell_1,\ell_2)$ with ℓ_2 even are on one side of $\mathbf{2}(\ell_1)$ and those with ℓ_2 odd are on the other. This ordering is inverted if ℓ_1 is odd. These remarks generalise to $\mathbf{n}$-modal orbits and lead to Definition 3.1.

All orbits so far computed have been located numerically on the local stable manifold and have been found there to be ordered relative to each other as described above (see Figure 14). In addition, the numerical evidence points to the existence for P close to -2, of orbits labelled by all possible symbol sequences. Such an ordering would imply many restrictions in the ways homoclinic orbits can bifurcate or coalesce, as explained in Section 6 below.

Note that, if the conjecture holds concerning the equivalence of the notation $[j_1,\ldots,j_{n-1}]$ and $\mathbf{n}(j_1,\ldots,j_{n-1})$, then, due to the reversibility and the 1-1 correspondence with symbolic dynamics, a symmetric homoclinic orbit must be labelled by a symmetric sequence. More generally, the image of an n-modal homoclinic orbit $\mathbf{n}(\ell_1, \ldots, \ell_{n-1})$ under the time-reversing transformation would be a homoclinic orbit with the reversed label $\mathbf{n}(\ell_{n-1}, \ldots, \ell_1)$.

The next section presents a numerical study of the persistence of multi-modal homoclinic orbits when P increases and tends to $P = 2$. Numerical computations, presented in (CHAMPNEYS & SPENCE, 1993; CHAMPNEYS & TOLAND, 1993), suggest that the primary and bi-modal orbit $\mathbf{2}(2)$ exist for all $P \in (-2, 2)$ and both bifurcate from 0 at $P = 2$ (a subcritical bifurcation). These results are not unexpected due to the work by Iooss and Pérouème (IOOSS & PEROUEME, 1993) concerning the existence of two homoclinic solutions for a reversible vector field in $\mathbb{R}^4$ near a 1:1 resonance. Their theory relies on a normal form approximation which can be applied to equation (1.1) (MIELKE, 1991). The approximated problem has two symmetric homoclinic solutions that persist in the full problem (here the reversibility is crucial). See also the calculations of Hunt *et al* (HUNT *et al.*, 1989; HUNT & WADEE, 1991).

No other branch of homoclinic orbits seems to reach $P = 2$. Rather they all seem to undergo coalescence (symmetric ones, for example) or subcritical bifurcation as described below. (The reader may wish to glance forward to Figure 24 for an illustration of the combined results of our numerical investigation.)

4 TRANSVERSALITY, COALESCENCE AND BIFURCATION FOR $P \in (-2, 2)$

This section is devoted to a coherent, though entirely heuristic explanation, in terms of the geometric theory of dynamical systems, of some interesting global phenomena which are observed for numerically calculated homoclinic orbits for $P > -2$. Analytic proofs in the precise context of equation (1.1) are beyond our present understanding.

4.1 Transversality

We give an account of what may happen to the infinite number of homoclinic orbits of (1.1) that exist for $P \in (-2, 2)$ ((BUFFONI, 1993a) gives a rigorous proof of the existence of some of them for $P \in (-2, 0)$), given that we do not expect any of the orbits to persist for $P > 2$. (For $P > 2$, the zero solution of (1.1) is a centre and Lyapunov's Centre Theorem gives the existence of infinitely many periodic solutions for such P. It is not known if homoclinic solutions exist for such P.) We view (1.1) as a dynamical system in

$\mathbb{R}^4$ with phase-space variables (u, u', u'', u''') where u satisfies (1.1). The dynamical system is reversible; specifically, it is invariant under the transformation

$$R: \ (u, u', u'', u''') \mapsto (u, -u', u'', -u'''), \quad t \mapsto -t. \tag{4.1}$$

We refer to the two-dimensional linear manifold of fixed-points of R as the *symmetric section*,

$$\Sigma = \left\{(a, b, c, d) \in \mathbb{R}^4 | \ b = d = 0\right\},$$

and let S and U denote the stable and unstable manifolds of 0 respectively. We suppose that $P \in (-\infty, 2)$, so that the stable and unstable manifolds are both two dimensional.

To establish what degeneracies may occur along a branch of homoclinic solutions, consider an arbitrary homoclinic orbit

$$\gamma = \{x(t) = (v(t), v'(t), v''(t), v'''(t)) : t \in \mathbb{R}\}. \tag{4.2}$$

Note that $0 \in \bar{\gamma} \backslash \gamma$. Since (3.1) is also Hamiltonian with total energy H, we know, due to standard transversality arguments, that if

$$S \text{ and } U \text{ intersect transversally in } H^{-1}(0) \text{ for some particular } P\text{-value}, \tag{4.3}$$

then the corresponding homoclinic orbit exists for all neighbouring P-values also and there is no bifurcation of homoclinic orbits from it. Recall, from Section 2, that (4.3) applied to (3.1) implies that, for each point $x(t)$ on the homoclinic orbit, the only common tangent direction to U and S is $x'(t) = (v'(t), v''(t), v'''(t), -Pv''(t) - v(t) + v^2(t))$. Such a transverse intersection between S and T is an open, or *codimension-zero*, phenomenon.

We shall now study what may happen when transversality defined by (4.3) fails as a generic parameter is varied in a four-dimensional Hamiltonian system that is invariant under (4.1) (i.e. in *codimension-one* situations for systems within this class). We shall consider symmetric and asymmetric homoclinic orbits separately. To that end we make the following definitions.

Definition *A homoclinic orbit is called* symmetric *if it intersects Σ. Then there is a unique choice of origin for t such that the homoclinic orbit $\gamma = \{x(t) : t \in \mathbb{R}\}$ satisfies $x(0) \in \Sigma$, and is invariant under (4.1). (If there were two distinct such time shifts, the orbit would be periodic, not homoclinic.) A homoclinic orbit is called* asymmetric *if it is not symmetric.*

4.2 Symmetric orbits : coalescence and symmetry-breaking bifurcation

Consider a *symmetric* homoclinic orbit γ given by (4.2) and suppose without loss of generality that its symmetric point occurs at $t = 0$, that is $x(0) \in \Sigma$. Note that if (4.3) fails we have that

$$T_{x(0)}S = T_{x(0)}U = T, \text{ say}, \tag{4.4}$$

since $H^{-1}(0)$ is 3-dimensional at $x(0)$. Note also that a symmetric homoclinic orbit persists as P is varied if

$$\text{at } x(0),\ U \text{ and } \Sigma \text{ intersect transversally in } \mathbb{R}^4, \text{ for some particular } P\text{-value}. \tag{4.5}$$

Unlike the case of (4.3), this refers to transversality in the full four-dimensional phase space. Note further that, for symmetric orbits, (4.3) implies (4.5). This is because if (4.5) fails then the tangent plane $T_{x(0)}U$ to U contains $(a, 0, b, 0)$ for some non-zero (a, b) and by reversibility $(a, 0, b, 0) \in T_{x(0)}S$ also. However, $x'(0) = (0, v''(0), 0, v''''(0)) \in T_{x(0)}U \cap T_{x(0)}S$ and so $T_{x(0)}U = T_{x(0)}S = T$.

For a general reversible system in $\mathbb{R}^4$ (i.e. a system satisfying (4.1) but which is not necessarily Hamiltonian) one has the following.

Lemma 4.1 *Given a symmetric homoclinic orbit $\gamma = \{x(t) : t \in \mathbb{R}\}$ of (1.1) with point of symmetry $x(0)$, that satisfies (4.4), then there exists $w \in \mathbb{R}^4$ such that $T = span\{x'(0), w\}$, $\|w\| = 1$, and either*

1. *$w \in \Sigma$ (i.e. $Rw = w$), or*
2. *$Rw = -w$.*

Proof This is immediate due to

$$T_{x(0)}U = RT_{x(0)}S$$

(see Section 2) and Section 4.3 of (CHAMPNEYS, 1994). □

Due to the Hamiltonian structure of the present example (4.4) implies that

$$T \subset \nabla H(x(0))^{\perp},$$

which means that, in case 1 of the preceding Lemma, $w \in \Sigma \cap \nabla H(x(0))^{\perp}$ (which it is one-dimensional since $x(0) \neq (0, 0, 0, 0)$). Therefore Lemma 4.1 yields (as was already derived in Section 2 for the primary symmetric orbit (see (2.3), (2.4)) two alternatives

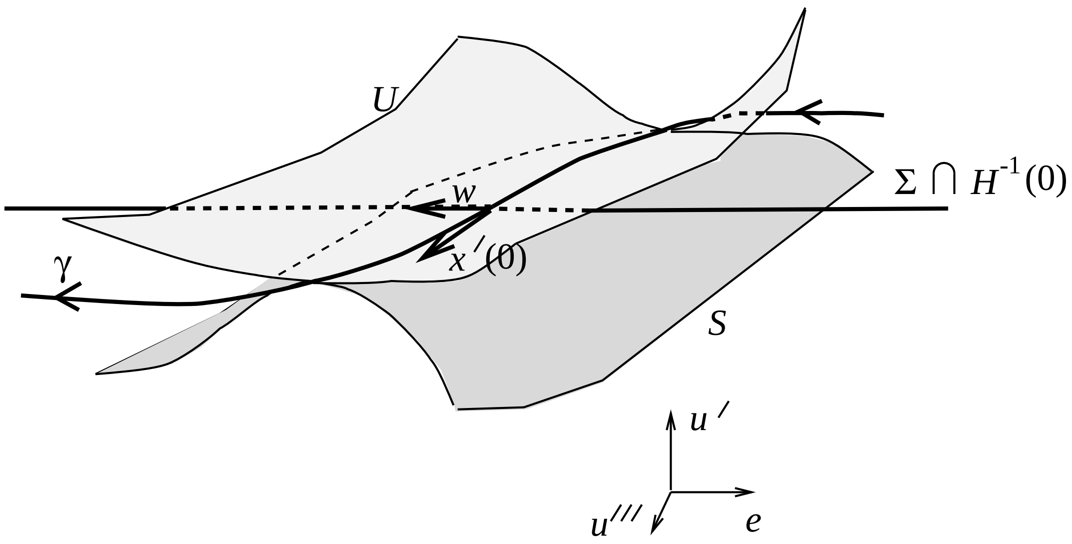

Figure 15: *Depicting the stable and unstable manifolds within $H^{-1}(0)$, in a neighbourhood of $x(0)$, intersecting according to case 1. Here e is a unit vector in the direction $(-v''(0), 0, v^2(0) - v(0), 0) \in \Sigma \cap \nabla H(x(0))^{\perp}$. A generic perturbation of the manifolds within $H^{-1}(0)$ in this case leads locally to either two homoclinic orbits or none at all.*

1. $T = \{(-av''(0), bv''(0), a(v^2(0) - v(0)), b(-Pv''(0) - v(0) + v^2(0))|a, b \in \mathbb{R}\}$

2. $T = \{(0, a, 0, b)|a, b \in \mathbb{R}\}$

We consider them separately.

Case 1. When 1 holds, the transversality condition (4.5) fails, since

$$T_{x(0)}U + \Sigma = T + \Sigma = \{(a, bv''(0), c, b(-Pv''(0) - v(0) + v^2(0))|a, b, c \in \mathbb{R}\} \cong \mathbb{R}^3 \ncong \mathbb{R}^4.$$

Generically, a non-transversal intersection between two smooth 2-dimensional manifolds in $\mathbb{R}^4$ implies a transition from zero to two one-dimensional intersections as a parameter is varied (a topological quadratic tangency). In the absence of extra symmetry or invariance properties, any other situation is of codimension two or higher. This analysis strongly suggests that in this case *two symmetric homoclinic orbits coalesce* and disappear as a parameter is varied (see Figure 15).

Case 2. Here T and Σ do intersect transversally in $\mathbb{R}^4$ and so a locally unique symmetric homoclinic orbit persists as P is varied. However, since we are supposing that (4.3) fails, S and T do not intersect transversally along $x(t)$ (within $H^{-1}(0)$), which non-transversality is generically broken upon varying a parameter. The situation must therefore be as depicted in Figure 16(a), where, due to (4.4), S and U have a topological cubic tangency at $x(0)$ (and hence at each point in $\{x(t)|t \in \mathbb{R}\}$.) Note, from Figure 16(b), that the reversibility forces the tangency to be odd, a generic perturbation of which results in the transition from one to three points of intersection. This suggests *the bifurcation of two asymmetric homoclinic orbits* from the primary symmetric one as a generic parameter is varied. Note further that the two bifurcating solutions are images of each other under (4.1).

4.3 Asymmetric orbits : coalescence

Consider the situation where U and S intersect non-transversally along an asymmetric homoclinic orbit $\{x(t) : t \in \mathbb{R}\}$, for example one of those which emanate from the bifurcation in Case 2 above. Since $\{x(t)|t \in \mathbb{R}\} \cap \Sigma = \emptyset$, there are no restrictions within $H^{-1}(0)$ for the tangent space

$$T = T_{x(0)}U = T_{x(0)}S$$

other than that it contains the vector $x'(0)$. The generic situation, then, is that there is a quadratic tangency between S and U, which implies a coalescence of homoclinic orbits, as in case 1 above, except that now it is the coalescence of a pair (x, y) of asymmetric homoclinic orbits which occurs. Note that $y \neq Rx$, otherwise at the coalescence $x = y = Rx$ would be a symmetric homoclinic orbit. In fact the pair (Rx, Ry) coalesce simultaneously and we conclude that there are two pairs of asymmetric homoclinic orbits coalescing at the same parameter value (which pairs are symmetrically related to each other).

Since quadratic tangency is generic, we conjecture that any *bifurcation* of homoclinic orbits from asymmetric homoclinic orbits (excluding bifurcations due to degeneracies in the linearisation about the origin — such as at $P = -2$) is of codimension two or higher.

4.4 Near simultaneous coalescence and bifurcation

The remainder of this section focuses on an entirely unexpected closeness of certain coalescence points and bifurcation points, detected numerically, offers an explanation in terms of the relative geometry of the stable and unstable manifolds and makes further inferences about this geometry which are then confirmed numerically in Section 5.

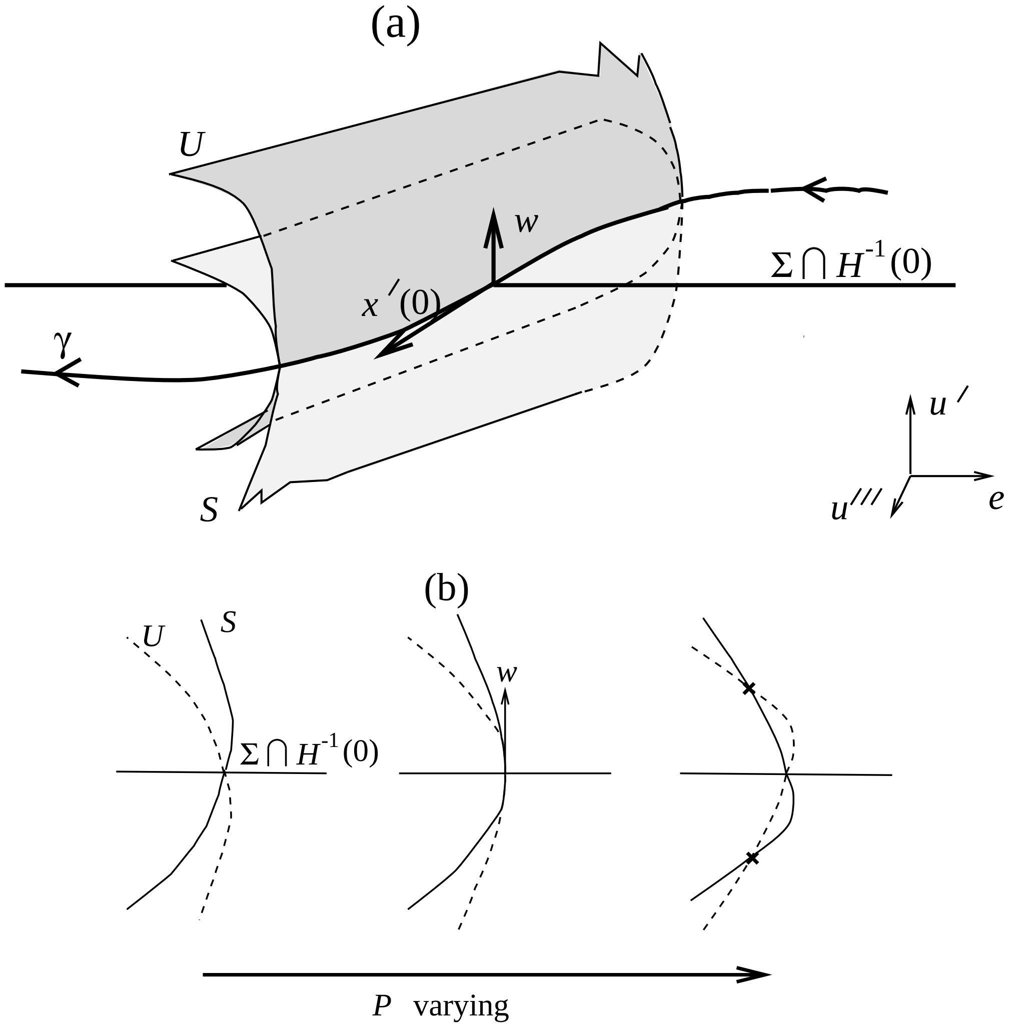

Figure 16: *(a) Depicting the stable and unstable manifolds within $H^{-1}(0)$, in a neighbourhood of $x(0)$, intersecting according to case 2 in the same co-ordinates as used in Figure 15. (b) Unfolding of the degeneracy in (a) under a generic perturbation within $H^{-1}(0)$, depicted in the Poincaré section plane span$\{w, \Sigma \cap H^{-1}(0)\}$.*

(a)

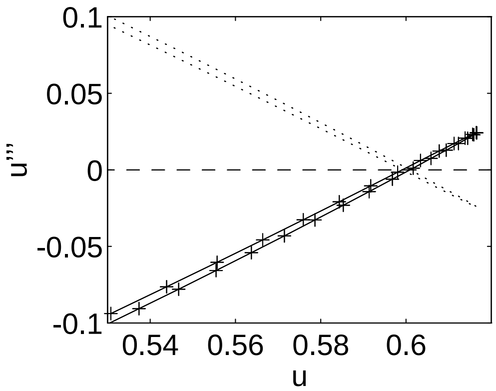

(b)

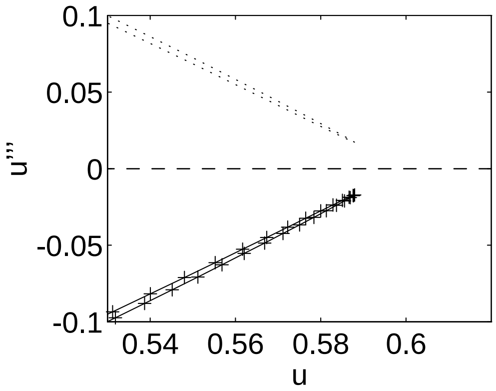

(c)

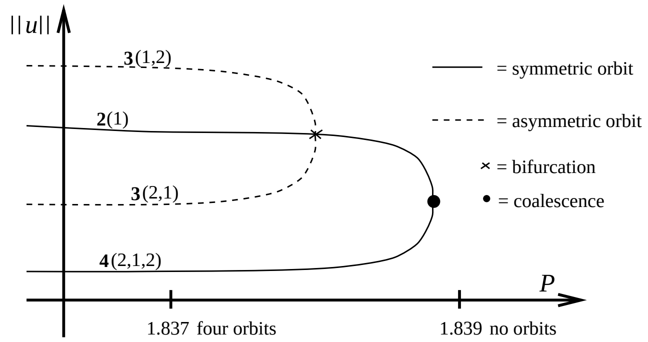

Figure 17: *Intersections of unstable manifold (solid line), stable manifold (dotted line) and the symmetric section (dashed line) for (a) $P = 1.837$ and (b) $P = 1.839$. (c) The corresponding bifurcation diagram for homoclinic orbits (drawn schematically), in which $||u||$ is used to denote a hypothetical norm of the solution.*

Figure 17(a) shows numerically computed stable and unstable manifolds in a neighbourhood of the $\mathbf{2}(1)$ bi-modal orbit for $P = 1.837$, plotted in (a projection of) the Poincaré section used in Figure 16(b). The existence of four homoclinic orbits, corresponding to the four intersection points between U and S, can be inferred from the figure. The two such intersections that occur on Σ correspond to symmetric homoclinic orbits and the two others to a symmetric pair of asymmetric orbits. Figure 17(b) shows the same portions of U and S for a slightly larger P-value. Note that all four orbits have now disappeared. The existence of two non-transversal symmetric homoclinic orbits for intervening P-values can be inferred, one corresponding to each of Cases 1 and 2 in Section 4.2. The bifurcation diagram is Figure 17(c), where the labels of the orbits involved in bifurcation and coalescence for this example are depicted.

Note, from Figure 17(a), that it is the "tentacle-like" geometry of the unstable manifold in a Poincaré section that gives rise to near simultaneous bifurcation and coalescence. If the portion of the unstable manifold concerned had been approximately flat near the symmetric section, then there would have been no secondary bifurcation near the coalescence. Intuitively one expects the unstable manifold to have (infinitely) many tentacles for P just greater than -2, due to the presence of Smale horseshoes. As P increases, the manifold begins to "unwrap itself". After a sufficient amount of unwrapping, the tentacles approach the symmetric section and the bifurcation sequence described above causes the destruction of two symmetric and two asymmetric homoclinic orbits. Furthermore, as P increases, other asymmetric orbits might be expected to disappear, by coalescence, when there is a tangency between a tentacle of the stable manifold and a tentacle of the unstable manifold away from the symmetric section. We suppose that this process continues until $P = 2$, by which point there are no longer any homoclinic orbits. A similar bifurcation sequence of *heteroclinic* orbits has been found to occur in the system describing travelling waves of the Kuramoto-Sivashinsky equation ((LAU, 1992)). To see the extent to which these qualitative ideas apply to the current model we turn now to numerical experiments.

5 THE GLOBAL PICTURE FOR $P \in (-2, 2)$: NUMERICAL RESULTS

The rest of the paper is devoted to an account of numerical results relating to the global behaviour, including bifurcation and coalescence, of branches of homomoclinic solutions for $P \in (-2, 2)$, and to a discussion of general principles which seem to emerge from these results.

5.1 Symmetric homoclinic orbits

The present Subsection is concerned exclusively with symmetric orbits. In earlier papers ((CHAMPNEYS, 1994; CHAMPNEYS & SPENCE, 1993; CHAMPNEYS & TOLAND, 1993)) branches of the primary and $\mathbf{2}(2)$ orbits were computed. Both were found to exist for all $P \in (-2, 2)$ and, for P close to 2, to be the orbits captured by the normal form analysis of (IOOSS & PEROUEME, 1993). A sample of other symmetric orbits were also computed, and it was found that they all disappear via coalescence (as described by case 1 in Section 4.2) at certain values of $P \in (1.5, 2)$. All these previous results were obtained using symmetric-section boundary conditions, which preclude the possibility of detecting bifurcations of asymmetric homoclinic orbits from symmetric ones. Here, to detect such bifurcations, we have repeated the previous calculations using full asymptotic boundary conditions. In addition, we have obtained more extensive results using symmetric-section boundary conditions and computed the loci of many more homoclinic orbits. For each branch computed using the former method, with the sole exception of the branch of primary and $\mathbf{2}(2)$ orbits, a similar bifurcation sequence to that described by Figure 17 was found, namely coalescence accompanied by bifurcation to asymmetric orbits. This mechanism seems always to account for the extinction of two branches of symmetric homoclinic orbits at some value of $P \in (1.5, 2.0)$. So far there is no numerical evidence for bifurcations from the primary or $\mathbf{2}(2)$ orbits for $P \in (-2, 2)$ or from the primary orbit for $P < -2$. Of course, the latter is impossible due to the uniqueness result in Section 2.

For convenience in what follows, we sometimes use the terms *orbits* and *branches* synonymously to mean a connected set of solutions, parameterised by $P \in (-2, P_c]$ and classified by their properties for P close to -2. To avoid confusion, we say that the pair of branches that are joined by coalescence at $P = P_c$ form a single homoclinic *locus* in a bifurcation diagram.

Tables 1–4 present the P-values of coalescence for certain orbits, as well as the label of the orbit with which coalescence occurs. The resulting pairs of orbit symbol sequences yield a label that represents a locus. We do not give the P-values of the nearby bifurcations to asymmetric orbits, because the difference between the bifurcation and the coalescence

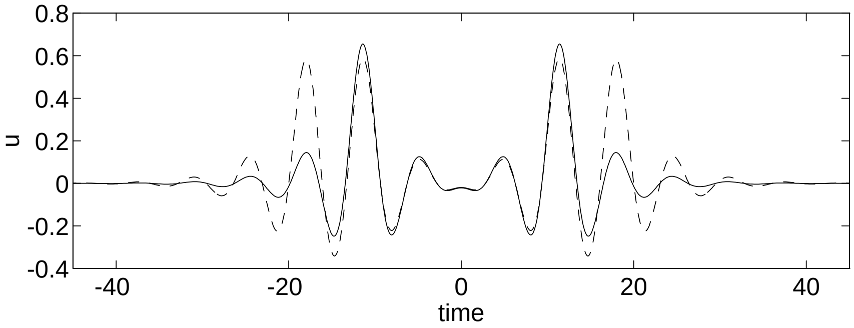

Figure 18: *Graphs of the orbits* $\mathbf{2}(7)$ *and* $\mathbf{4}(2,7,2)$ *at* $P = 1.8$

P-values for each orbit presented was found to be in the 5th or 6th decimal place, and at the limit of the accuracy of the numerical calculations.

Label	*P-value*	*Coalescent orbit*
primary	2.0	-
2(1)	1.83817	**4**(2,1,2)
2(2)	2.0	-
2(3)	1.90727	**4**(2,3,2)
2(4)	1.79047	**3**(2,2)
2(5)	1.92412	**4**(2,5,2)
2(6)	1.86001	**4**(2,2,2)
2(7)	1.93328	**4**(2,7,2)
2(8)	1.89615	**4**(2,4,2)

Label	*P-value*	*Coalescent orbit*
2(9)	1.93973	**4**(2,9,2)
2(10)	1.91738	**4**(2,6,2)
2(11)	1.94485	**4**(2,11,2)
2(12)	1.93096	**4**(2,8,2)
2(13)	1.94915	**4**(2,13,2)
2(14)	1.94022	**4**(2,10,2)
2(15)	1.95286	**4**(2,15,2)
2(16)	1.95618	**4**(2,12,2)
2(17)	1.95608	**4**(2,17,2)

Table 1: *Coalescence of bi-modal orbits*

An important question still to be addressed is the relationship, if any, between the two symbol sequences of a locus. Since each branch seems to coalesce with exactly one other branch it is natural to ask if there is some rule that governs the labels of the two orbits which coalesce to form a locus. A related question is to determine the *ordering* of the coalescence with respect to P. To begin with here are some observations from the numerical data.

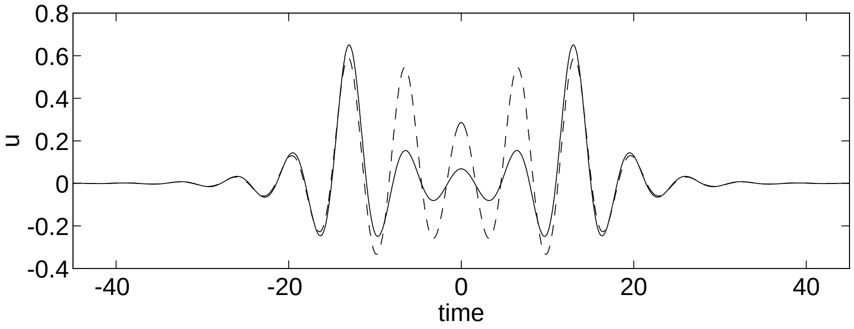

Figure 19: *Graphs of the orbits* $\mathbf{2}(8)$ *and* $\mathbf{4}(2,4,2)$ *at* $P = 1.8$

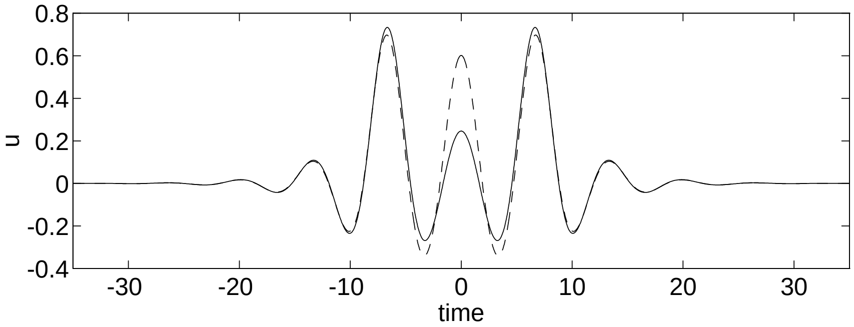

Figure 20: *Graphs of the orbits* $\mathbf{2}(4)$ *and* $\mathbf{3}(2,2)$ *at* $P = 1.7$

Note, that in Table 1, all bi-modal orbits with label $\mathbf{2}(k)$, k odd, coalesce with 4-modal orbits whose label is $\mathbf{4}(2,k,2)$ and all bi-modal orbits with label $\mathbf{2}(k+2)$, k even, coalesce with $\mathbf{4}(2,k-2,2)$. The case of $\mathbf{2}(4)$ coalescing with $\mathbf{3}(2{,}2)$ requires the identification of the symbol 0 with the lack of a symbol. Thus we seem to have the rule

$$(2i-1) \leftrightarrow (2,2i-1,2), \quad (2i+2) \leftrightarrow (2,2i-2,2), \quad i = 1,\ldots\infty, \tag{5.1}$$

where, for convenience, the bold face character in front of a symbol sequence has been omitted. That this rule may be a natural metamorphosis is suggested by Figures 18–20 which may be interpreted as follows. Figure 18 shows an example of two orbits (a bi-modal and a 4-modal) with odd middle symbols, on the same homoclinic locus and at the same P-value, which obey the rule. As P is increased the largest "oscillations" in the tail (in practice for $\mathbf{2}(2k-1)$ orbits these are the maxima outside the region between the humps which are attained closest to a hump) of the bi-modal orbit grows into a new "hump" as one follows the locus around the coalescence point. Since the orbit is symmetric, two extra humps must be formed in this process and a bi-modal orbit becomes 4-modal. By contrast, for a bi-modal orbit with even symbol (> 2), it seems always to be the *global-local maximum between* the two humps that grows to form an additional hump (Figure 19). (Here the global-local maximum means the global maximum of $u(t)$ in the t-interval when the path is in $\mathcal{N}$, between consecutive humps where maxima are attained.) Provided this largest oscillation is not in the middle (i.e the global-local maximum of u in question is not the symmetric point) then two extra humps are formed by this process. Note that if the path spirals inwards then the $\mathbf{2}(2k)$ orbit will have its global-local maximum between the humps at a path point on the first wind around 0 (see Figures 5 and 12). Except in the case $k = 2$ this is not the symmetric point of the orbit ($\mathbf{2}(2)$ has no global-local maximum between its two humps.) For the $\mathbf{2}(4)$ orbit (Figure 20), however, there is only one oscillation between the two humps, which oscillation necessarily contains the symmetric point. The (single) oscillation containing the point of symmetry grows into a hump and this bi-modal orbit becomes tri-modal on passing around the coalescence point on the homoclinic locus.

Note also, from Table 1, a general pattern that bi-modal orbits with numerically larger symbols appear to coalesce at higher values of P. In fact, upon considering separately the bi-modal orbits with even symbols and with odd symbols, one observes two numerically increasing sequences of coalescence P-values converging towards $P = 2$. Note that a theoretical explanation of these observations is offered in Section 6; see (P1)–(P4) and the ensuing discussion.

Label	*P-value*	*Coalescent orbit*
3(1,1)	1.83375	**5**(2,1,1,2)
3(2,2)	1.79047	**2**(4)
3(3,3)	1.90561	**5**(2,3,3,2)
3(4,4)	1.80518	**5**(2,2,2,2)

Label	*P-value*	*Coalescent orbit*
3(5,5)	1.92304	**5**(2,5,5,2)
3(6,6)	1.86618	**5**(2,4,4,2)
3(7,7)	1.93237	**5**(2,7,7,2)
3(8,8)	1.90001	**5**(2,6,6,2)

Table 2: *Coalescence of tri-modal symmetric homoclinic orbits*

Now consider the tri-modal orbits (Table 2). Here, the behaviour of the second symbol at coalescence must be identical to that of the first symbol due to symmetry. More generally, for any symmetric homoclinic orbit with modality greater than two, the second half of its symbol sequence must be the reverse of the first half. Accordingly, when attempting to understand the coalescence of symmetric homoclinic orbits, we need only consider strings of symbols up to their symmetric points; the behaviour of the latter half being fixed by reversibility. Note that, with the exception of $\mathbf{3}(2,2)$, all the tri-modals presented obey the rule

$$(2i+1, 2i+1) \leftrightarrow (2, 2i+1, 2i+1, 2), \quad (2i+2, 2i+2) \leftrightarrow (2, 2i, 2i, 2), \quad i = 0, \ldots \infty, \quad (5.2)$$

and that this rule is similar to rule (5.1) for bi-modals except that 2 rather than 4 is subtracted from the even symbols; (e.g. $(8,8) \leftrightarrow (2,6,6,2)$ whereas $(8) \leftrightarrow (2,4,2)$, *cf.* Figures 20 and 21). This is because the position of the symmetric point affects the possible coalescence of bi-modal and tri-modal orbits whose labels consist of even symbols. Specifically, for a bi-modal orbit $\mathbf{2}(2i+2)$, the even symbol necessarily occurs in the middle and so neither of the transformations $2i+2 \leftrightarrow 2, 2i$, or $2i+2 \leftrightarrow 2i, 2$, that occur for the first and second symbols respectively of the tri-modal orbit $\mathbf{3}(2i+2, 2i+2)$, can occur due to symmetry. The one exception to (5.2) is **3**(2,2), but this was accounted for by coalescence with **2**(4). Similarly, **2**(2) was not considered in (5.1) as this orbit had already been found to exist for all $P \in (-2, 2)$. Accordingly, we propose a scheme for investigating these matters:

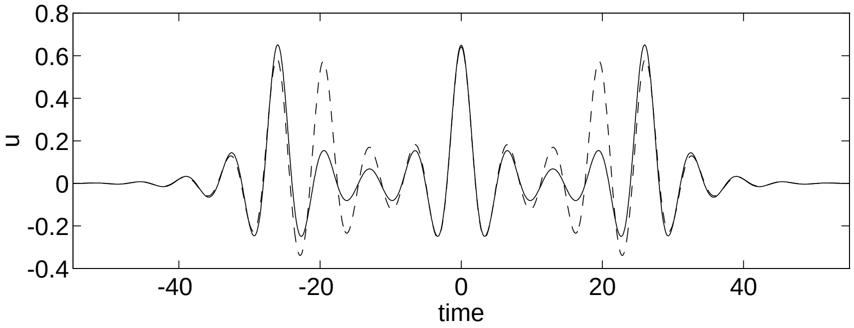

Figure 21: *Graphs of the orbits* $\mathbf{3}(8,8)$ *and* $\mathbf{5}(2,6,6,2)$ *at* $P=1.8$

systematically examine examples from the (infinite) list of symmetric homoclinic orbits in the following order — first the primary and $\mathbf{2}(2)$, then the rest of the bi-modals, then the tri-modals, 4-modals, etc... — and at each step, strike from future consideration all orbits whose coalescence with one of the present modality has been noted.

Observe further, from Table 2, that, as with bi-modals, the P-values of coalescence of tri-modal orbits represent two increasing sequences, one for orbits with both symbols even and equal and one for those with both symbols equal and odd. This is compatible with (P1) – (P4) of Section 6.

In Table 3, results are presented on several sequences of 4-modal orbits. Consider the first two sequences presented, $4(1,*,1)$ and $4(3,*,3)$, for which the outer symbols are odd (note that we do not need to consider $4(2,*,2)$ because these are all accounted for via coalescence with bi-modals). Numerically, the observed orbits obey the following generalisation of (5.1):

$$\begin{aligned} (\mathbf{k},j,\mathbf{k}) &\leftrightarrow (2,\mathbf{k},j,\mathbf{k},2), \text{ if } j \text{ is odd} \\ (\mathbf{k},j+2,\mathbf{k}) &\leftrightarrow (\mathbf{k},2,j-2,2,\mathbf{k}), \text{ if } j+2 \text{ is even,} \end{aligned} \tag{5.3}$$

where $\mathbf{k}$ is any sequence composed of 2's and odd numbers only.

We have not found any evidence of this rule being violated; furthermore, we have found no examples of any *odd* symbols in the symbol sequence of a symmetric homoclinic orbit changing at a coalescence point. We have yet to consider a rule for the orbit $\mathbf{4}(1,2,1)$, but note that it behaves according to (5.3) with 2 behaving as an odd number. In fact, we

Label	*P-value*	*Coalescent orbit*
4(1,1,1)	1.83346	**6**(2,1,1,1,2)
4(1,2,1)	1.83891	**6**(2,1,2,1,2)
4(1,3,1)	1.83737	**6**(2,1,3,1,2)
4(1,4,1)	1.68794	**5**(1,2,2,1)
4(1,5,1)	1.83784	**6**(2,1,5,1,2)
4(1,6,1)	1.77948	**6**(1,2,2,2,1)
4(1,7,1)	1.83800	**6**(2,1,7,1,2)
4(1,8,1)	1.81799	**6**(1,2,4,2,1)
4(3,1,3)	1.90035	**6**(2,3,1,3,2)
4(3,2,3)	1.90824	**6**(2,3,2,3,2)
4(3,3,3)	1.90553	**6**(2,3,3,3,2)
4(3,4,3)	1.76985	**5**(3,2,2,3)
4(3,5,3)	1.90638	**6**(2,3,5,3,2)
4(3,6,3)	1.80485	**6**(3,2,2,2,3)
4(3,7,3)	1.90672	**6**(2,3,7,3,2)
4(3,8,3)	1.87573	**6**(3,2,4,2,3)
4(4,1,4)	1.72896	**6**(2,2,1,2,2)
4(4,2,4)	1.81501	**6**(2,2,2,2,2)
4(4,3,4)	1.77958	**6**(2,2,3,2,2)
4(4,4,4)	1.80005	**6**(2,2,4,2,2)
4(4,5,4)	1.78770	**6**(2,2,5,2,2)
4(4,6,4)	1.79215	**6**(2,2,6,2,2)
4(4,7,4)	1.78978	**6**(2,2,7,2,2)
4(4,8,4)	1.79082	**6**(2,2,8,2,2)

Label	*P-value*	*Coalescent orbit*
4(5,1,5)	1.91557	**6**(2,5,1,5,2)
4(5,2,5)	1.92502	**6**(2,5,2,5,2)
4(5,3,5)	1.92207	**6**(2,5,3,5,2)
4(5,4,5)	1.78489	**5**(5,2,2,5)
4(5,5,5)	1.92300	**6**(2,5,5,5,2)
4(5,6,5)	1.85312	**6**(5,2,2,2,5)
4(5,7,5)	1.92339	**6**(2,5,7,5,2)
4(5,8,5)	1.88744	**6**(5,2,4,2,5)
4(6,1,6)	1.80239	**6**(4,2,1,2,4)
4(6,2,6)	1.87533	**6**(2,4,2,4,2)
4(6,3,6)	1.84906	**6**(4,2,3,2,4)
4(6,4,6)	1.79421	**5**(6,2,2,6)
4(6,5,6)	1.85642	**6**(4,2,5,2,4)
4(6,6,6)	1.86400	**6**(2,4,6,4,2)
4(6,7,6)	1.85878	**6**(4,2,7,2,4)
4(6,8,6)	1.86089	**6**(2,4,8,4,2)
4(8,1,8)	1.82765	**6**(6,2,1,2,6)
4(8,2,8)	1.90700	**6**(2,6,2,6,2)
4(8,3,8)	1.88231	**6**(6,2,3,2,6)
4(8,4,8)	1.79123	**5**(8,2,2,8)
4(8,5,8)	1.89110	**6**(6,2,5,2,6)
4(8,6,8)	1.86196	**6**(8,2,4,2,8)
4(8,7,8)	1.89410	**6**(6,2,7,2,6)
4(8,8,8)	1.89861	**6**(2,6,8,6,2)

Table 3: *Coalescence of* 4*-modal symmetric homoclinic orbits*

have found no example of the symbol 2 in the symbol sequence of a symmetric homoclinic orbit of any modality changing at a coalesce point (other than to become an orbit of *lower* modality). Observe, for example from Figure 21, the distinction in the graph of an orbit between "2" and other even symbols. A symbol "2" represents a half oscillation and so there is no corresponding global-local maximum whereas all other even symbols represent at least one full oscillation and thus there is a global-local maximum. In what follows we shall partition the positive integers according to whether the above discussion suggests the corresponding symbol can change or not at coalescence:

$$\textit{changeable} \Rightarrow 4, 6, 8 \ldots, \qquad \textit{unchangeable} \Rightarrow 1, 2, 3, 5, 7 \ldots.$$

Hence we have

$$(\mathbf{k}, j, \mathbf{k}) \quad \leftrightarrow \quad (2, \mathbf{k}, j, \mathbf{k}, 2), \text{ if } j \text{ is unchangeable} \tag{5.4}$$

$$(\mathbf{k}, j+2, \mathbf{k}) \quad \leftrightarrow \quad (\mathbf{k}, 2, j-2, 2, \mathbf{k}), \text{ if } j+2 \text{ is changeable} \tag{5.5}$$

where $\mathbf{k}$ is any sequence composed of unchangeable numbers only.

Observe, from the rest of Table 3 (sequences **4**(4,*,4) **4**(5,*,5) **4**(6,*,6) and **4**(8,*,8)), that some further patterns can be spotted. Firstly the coalescent orbit is always obtained by either altering a single changeable symbol (up to symmetry) or, if all symbols are unchangeable, by adding 2's either side according to (5.4). In the former situation, it is always the smallest changeable symbol that is changed whenever this is uniquely defined (up to symmetry). If this unique smallest changeable symbol is a middle symbol, it obeys rule (5.5)

where $\mathbf{k}$ is composed of symbols that are either unchangeable or $> j+2$ and changeable. (5.6)

If there is a unique smallest symbol (up to symmetry) in the symbol sequence and it is not in the middle, then we have a new rule that is a generalisation of (5.2):

$$(\mathbf{k}, j, \mathbf{l}, j, \mathbf{k}) \leftrightarrow \begin{cases} \text{either} & (\mathbf{k}, j-2, 2, \mathbf{l}, 2, j-2, \mathbf{k}) \\ \text{or} & (\mathbf{k}, 2, j-2, \mathbf{l}, j-2, 2, \mathbf{k}) \end{cases}, \quad \text{where } j \text{ is changeable} \tag{5.7}$$

and $\mathbf{k}, \mathbf{l}$ are composed of symbols that are unchangeable or $> j$ and changeable; $\mathbf{l}$ is symmetric.

Note that there is an indeterminacy in (5.7) and at present it is not clear how to decide which of the two alternatives occur (compare, for example, the coalescences of **4**(6,7,6) and **4**(6,8,6)).

We have yet to consider symbol sequences in which the smallest changeable entry is not unique (up to symmetry). The three examples of such examples of such in Table 3 (**4**$(4,4,4)$, **4**$(6,6,6)$ and **4**$(8,8,8)$) are all orbits with three identical symbols and it is the first symbol that changes at coalescence (but look ahead to **8**$(4,4,1,4,1,4,4)$ in Table 4).

Finally, observe from Table 3 that the coalescence P-values of the presented sequences are consistent with two ultimately increasing sequences which converge to different limits. In the case of the sequence **4**(3,*,3), computations not tabulated here suggest that the P-values of coalescence of orbits with odd middle symbol converge to $P \approx 1.907$ (e.g. **4**(3,13,3) coalesces at $P = 1.90712$), and those with even middle symbol to converge to $P \approx 1.905$ (e.g. **4**(3,14,3) coalesces at $P = 1.90495$). Recall that **4**(2,3,2) and **2**(3) coalesce at $P = 1.90727$, and that **3**(3,3) and **5**(2,3,3,2) coalesce at $P = 1.90561$.

Label	*P-value*	*Coalescent orbit*
5(3,1,1,3)	1.89999	**7**(2,3,1,1,3,2)
5(3,2,2,3)	1.76985	**4**(3,4,3)
5(3,3,3,3)	1.90552	**7**(2,3,3,3,3,2)
5(3,4,4,3)	1.79113	**7**(3,2,2,2,2,3)
5(3,5,5,3)	1.90641	**7**(2,3,5,5,3,2)
5(3,6,6,3)	1.85256	**7**(3,2,4,4,2,3)
6(1,6,1,6,1)	1.77956	**8**(1,2,4,1,4,2,1)
6(1,6,2,6,1)	1.80663	**8**(1,2,4,2,4,2,1)
6(1,6,3,6,1)	1.79949	**8**(1,2,4,3,4,2,1)
6(2,4,5,4,2)	1.81989	**8**(2,2,2,5,2,2,2)
6(3,2,1,2,3)	1.90049	**8**(2,3,2,1,2,2,3)
6(3,2,2,2,3)	1.84085	**4**(3,6,3)
6(3,2,3,2,3)	1.90822	**8**(2,3,2,3,2,3,2)
6(3,1,8,1,3)	1.81754	**8**(3,1,2,4,2,1,3)
6(3,8,1,8,3)	1.82671	**8**(3,6,2,1,2,6,3)

Label	*P-value*	*Coalescent orbit*
6(4,4,1,4,4)	1.73220	**8**(4,2,2,1,2,2,4)
6(6,6,5,6,6)	1.86005	**8**(6,4,2,5,2,4,6)
6(6,6,6,6,6)	1.86418	**8**(2,4,6,6,6,4,2)
6(6,6,7,6,6)	1.86326	**8**(6,4,2,7,2,4,6)
6(8,6,7,6,8)	1.85965	**8**(8,4,2,7,2,4,8)
6(6,6,8,6,6)	1.86489	**8**(2,4,6,8,6,4,2)
6(8,6,8,6,8)	1.86189	**8**(8,4,2,8,2,4,8)
6(8,6,9,6,8)	1.86052	**8**(8,4,2,9,2,4,8)
6(8,6,10,6,8)	1.86121	**8**(8,4,2,10,2,4,8)
8(1,4,4,4,4,4,1)	1.73188	**10**(1,2,2,4,4,4,2,2,1)
8(4,1,4,1,4,1,4)	1.68817	**10**(4,1,2,2,1,2,2,1,4)
8(4,1,4,4,4,1,4)	1.72892	**10**(2,2,1,4,4,4,1,2,2)
8(4,4,1,4,1,4,4)	1.68812	**9**(4,4,1,2,2,1,4,4)
8(8,2,4,8,4,2,8)	1.83016	**10**(8,2,2,2,8,2,2,2,8)

Table 4: *Miscellaneous symmetric homoclinic orbits*

Table 4 presents the coalescence properties of certain miscellaneous higher-modal

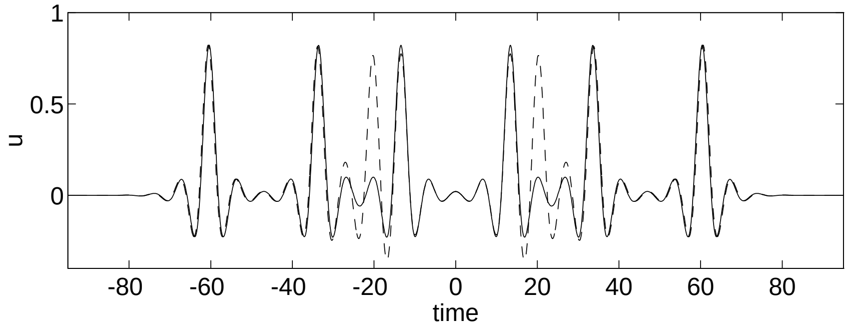

Figure 22: *Graphs of the orbits* $\mathbf{6}(8,6,8,6,8)$ *and* $\mathbf{8}(8,4,2,8,2,4,8)$ *at* $P = 1.6$

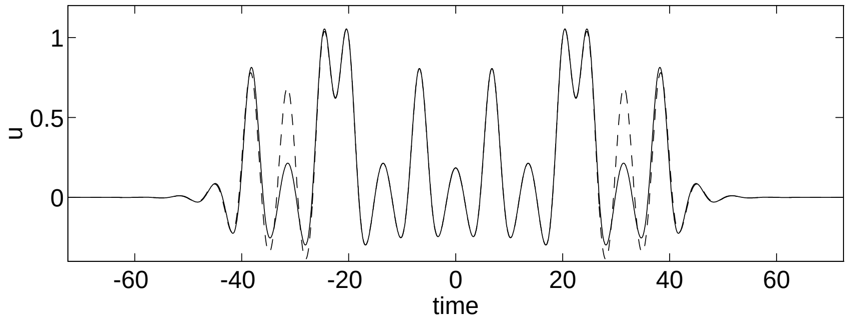

Figure 23: *Graphs of the orbits* $\mathbf{8}(4,1,4,4,4,1,4)$ *and* $\mathbf{10}(2,2,1,4,4,4,1,2,2)$ *at* $P = 1.6$

orbits, two of which are presented in Figures 22 and 23. Note that all these data are consistent with the rules so far proposed, but that no clear pattern emerges concerning the two so far undecided situations: namely, which alternative of (5.7) should apply and which of a multiplicity of smallest changeable symbols should be the one to change. In the former case, contrast the behaviour of **6**(8,6,7,6,8) and **6**(8,6,8,6,8), presented in Table 4, with that of **4**(6,7,6) and **4**(6,8,6), presented in Table 3. For the latter, consider the four next-to-last orbits presented in the second column of Table 4. Here it sometimes the first, and sometimes the last (i.e. closest to middle) occurrence of the symbol 4 that is transformed at coalescence.

It is possible that some resolution of these uncertainties will become apparent upon computing orbits of higher modality. Note, however, from Figures 22 and 23, that the orbits already computed require solving a boundary-value problem over a significantly long time-interval to approach the limit of what can practically be continued using current

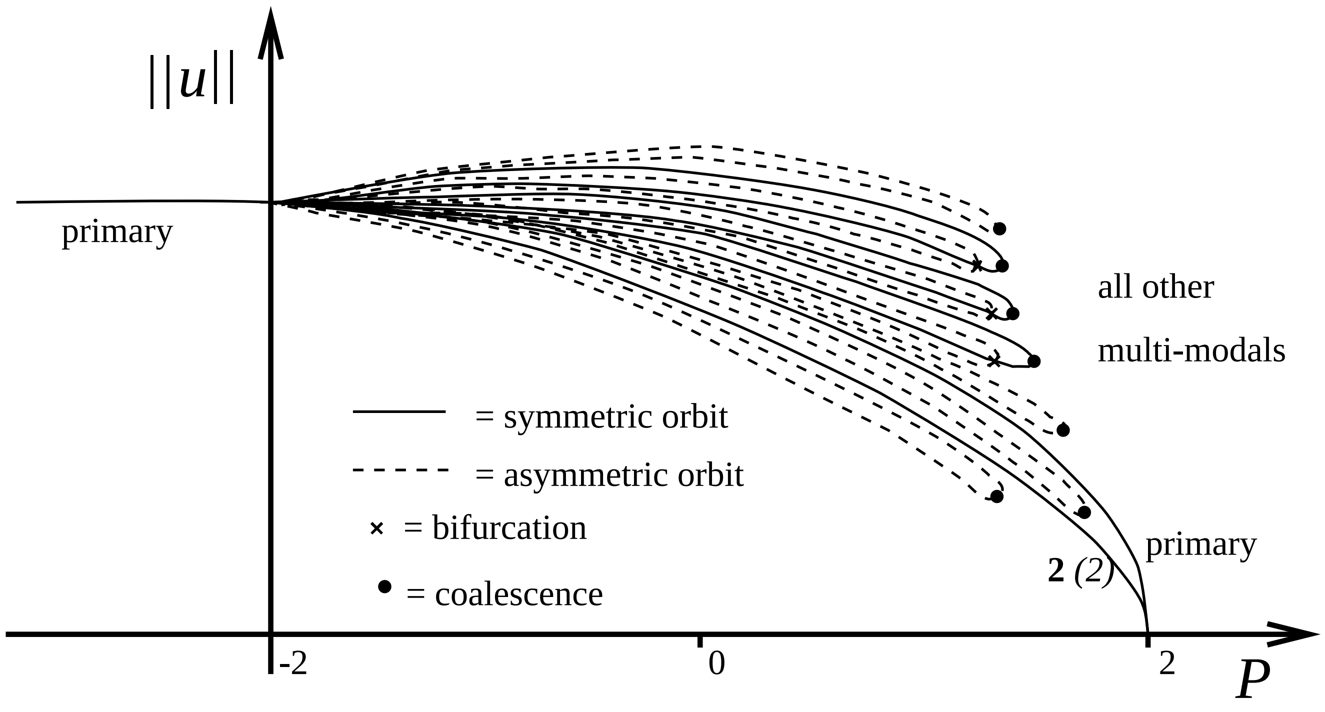

Figure 24: *Schematic bifurcation diagram of homoclinic orbits.*

techniques.

5.2 Asymmetric homoclinic orbits: numerical results

Here we present new results on the continuation of asymmetric homoclinic orbits, using AUTO with full asymptotic boundary conditions. Each asymmetric orbit computed originally at $P = 1.5$ was found to either coalesce for some $P \in (1.5, 2)$ or to disappear via a bifurcation from a symmetric homoclinic orbit. We have found that all such bifurcations occur near the coalescence point of a symmetric homoclinic orbit (as described in Section 4.4), and have found no evidence at all of bifurcation of orbits from asymmetric homoclinic orbits. Figure 24 presents schematically what we now believe to be the global bifurcation diagram for homoclinic orbits of (3.1).

Tables 5 and 6 present the P-values at which certain 3- and 4-modal asymmetric orbits disappear. For those orbits that disappear via coalescence we indicate, in the third column of the tables, the other orbit involved. For those that disappear by bifurcation we give, in the third and forth columns respectively, the other bifurcating orbit and the symmetric orbit from which bifurcation occurs. Thus coalescence or bifurcation is indicated by whether or not the fourth column is blank. Figures 25 – 27 show graphs of

Label	*P-value*	*Coalescent orbit*	*Bifurcation from*
3(1,2)	1.83817	**3**(2,1)	**2**(1) or **4**(2,1,2)
3(1,3)	1.83751	**4**(2,1,3)	-
3(1,4)	1.72875	**4**(1,2,2)	-
3(1,5)	1.83790	**4**(2,1,5)	-
3(1,6)	1.80226	**4**(1,2,4)	-
3(2,1)	1.83817	**3**(1,2)	**2**(1) or **4**(2,1,2)
3(2,3)	1.90718	**3**(3,2)	**2**(3) or **4**(2,3,2)
3(2,4)	1.83002	**3**(4,2)	**2**(6) or **4**(2,2,2)
3(2,5)	1.92391	**3**(5,2)	**2**(5) or **4**(2,5,2)
3(2,6)	1.88430	**3**(6,2)	**2**(8) or **4**(2,4,2)
3(3,1)	1.83751	**4**(3,1,2)	-
3(3,2)	1.90718	**3**(2,3)	**2**(3) or **4**(2,3,2)
3(3,4)	1.77930	**4**(3,2,2)	-
3(3,5)	1.90643	**4**(2,3,5)	-
3(3,6)	1.84867	**4**(3,2,4)	-

Table 5: *Asymmetric tri-modal orbits; see text for explanation*

examples from both tables. There now follow a few observations comparing these results with symmetric coalescence.

The asymmetric orbits that bifurcate near a symmetric coalescence are a symmetric pair (see Section 4.2). The numerical results suggest that the labels of all asymmetric orbits emanating from a bifurcation may be obtained by performing "half" the symbol-transformation to the lower-modal symmetric orbit that gives its coalescent partner. For example, observe from Table 6 that the orbit **4**(2,2,4) bifurcates from (one of) the coalescent pair **3**(4,4) and **5**(2,2,2,2). For those asymmetric orbits which coalesce, rather than originating in a bifurcation, the behaviour of the orbit with the reversed symbol is implied by the reversibility (as predicted in Section 4.3). For example, observe, from Table 5, that the orbits with labels **3**(1,3) and **3**(3,1), which are a symmetric pair, coalesce at the same value of P with orbits having the symmetrically related labels **4**(2,1,3) and **4**(3,1,2)

Label	*P-value*	*Coalescent orbit*	*Bifurcation from*
4(2,1,1)	1.83341	**4**(1,1,2)	**3**(1,1) or **5**(2,1,1,2)
4(2,1,3)	1.83750	**3**(1,3)	-
4(2,1,4)	1.72911	**5**(2,1,2,2)	-
4(2,1,5)	1.83790	**3**(1,5)	-
4(2,1,6)	1.80251	**5**(2,1,2,4)	-
4(2,2,1)	1.72875	**3**(4,1)	-
4(2,2,3)	1.77930	**3**(4,3)	-
4(2,2,4)	1.80380	**4**(4,2,2)	**3**(4,4) or **5**(2,2,2,2)
4(2,2,5)	1.78758	**3**(4,5)	-
4(2,2,6)	1.79227	**3**(4,6)	-
4(3,1,1)	1.83370	**5**(3,1,1,2)	-
4(3,1,2)	1.83751	**3**(3,1)	-
4(3,1,3)	1.90035	**6**(2,3,1,3,2)	-
4(3,1,4)	1.72849	**5**(3,1,2,2)	-
4(3,2,1)	1.90044	**5**(3,2,1,2)	-
4(3,2,2)	1.77930	**3**(3,4)	-
4(3,2,4)	1.84887	**3**(3,6)	-

Table 6: *Analogous to the previous table, but for 4-modal orbits.*

respectively. Moreover, the relationships between symbol sequences of coalescent orbits appear to follow rules analogous to those for symmetric coalescence, with the obvious differences due to the lack of symmetry. For example, observe from Tables 5 and 6 that a symbol 2 is placed *either* before *or* after a string consisting entirely of unchangeable symbols (compare, for example, **3**(3,1) and **3**(3,5) illustrated in Figures 25 and 26). Also, those containing changeable symbols appear to obey a rule similar to (5.7) (e.g. **4**(2,1,6), illustrated in Figure 27).

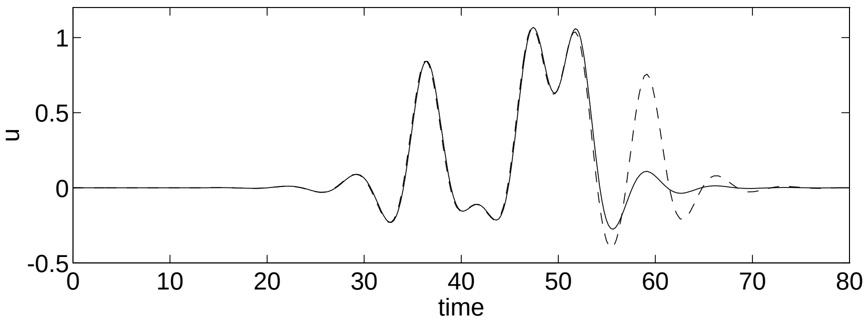

Figure 25: *Graphs of the orbits* $\mathbf{3}(3,1)$ *and* $\mathbf{4}(3,1,2)$ *at* $P = 1.6$

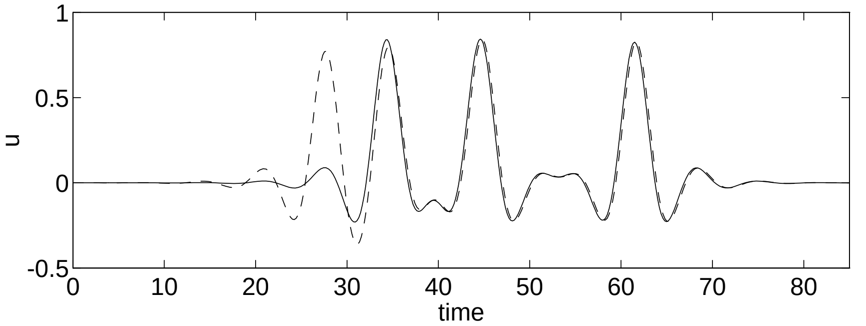

Figure 26: *Graphs of the orbits* $\mathbf{3}(3,5)$ *and* $\mathbf{4}(2,3,5)$ *at* $P = 1.6$

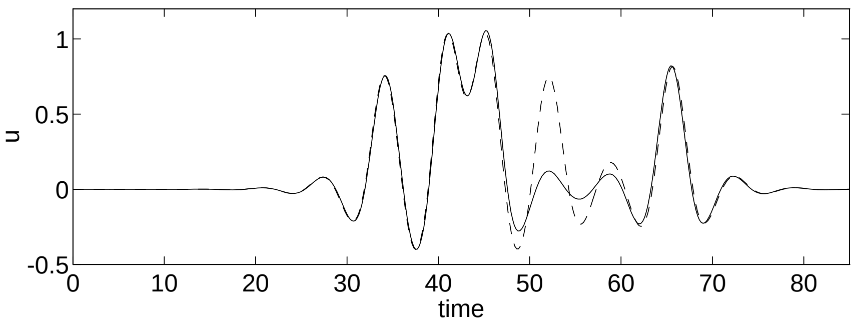

Figure 27: *Graphs of the orbits* $\mathbf{4}(2,1,6)$ *and* $\mathbf{5}(2,1,2,4)$ *at* $P = 1.6$

6 DISCUSSION

Here we examine various conjectures, made in Section 5.1 above, concerning rules for coalescence of symmetric homoclinic orbits, while avoiding the harder question concerning the coalescence of asymmetric orbits (although clearly the two problems are related). Some sketchy theoretical justification of the conjectured rules is motivated. Many open questions remain, but the rules we have observed are at least consistent with certain general principles that one can derive from the properties of (3.1) and in many cases represent the simplest among many alternatives.

In seeking a theoretical basis for our empirical rules, look first at which orbits *cannot* coalesce. There are essentially two mechanisms which preclude coalescence between specific orbits. The first concerns the geometric properties of intersections between the paths of homoclinic orbits and the set $\{W = 0\}$ (recall the definition of W in Section 3.2). The second concerns the ordering of orbits in the (two-dimensional) unstable manifold U, see Definition 3.1.

Note, from the geometric construction in Section 3.1, that paths of symmetric homoclinic orbits have their symmetric homoclinic points on $\{W = 0\}$. Moreover, for P near -2 and n even, all points of symmetry of n-modal orbits lie within a small neighbourhood of 0 on one of the four rays Σ_0, Σ_1, Σ_2 or Σ_3. To be more precise, the symmetric point lies on Σ_i, $i = \ell_{n/2} \pmod 4$, where $\ell_{n/2}$ is the middle symbol of the orbit. Note that, by the classical uniqueness result for initial value problems, it is not possible for a symmetric homoclinic point to pass though 0 in q-space and that, in a neighbourhood of 0, Σ_2 and Σ_3 are disjoint branches of $\{W = 0\} \setminus 0$. Recall the numerical observation that the primary orbit exists for all $P \in [-2, 2)$ and that the symmetric homoclinic point of the primary orbit lies between B and C on $\partial\Omega$. If we assume that the primary branch does not coalesce, then we can conclude that a symmetric homoclinic point on a given Σ_i must remain there as P is varied along a homoclinic orbit. *This implies that if the middle symbol of a symmetric homoclinic orbit changes at coalescence, then it must change by a multiple of four* (cf. rule (5.5)).

Another consequence of the geometrical construction is that the path of an orbit cannot change the number of its intersections with the set $\{W = 0\}$, while remaining bounded (provided we regard a crossing of $\{W = 0\}$ at zero or with zero velocity as two intersections and we disregard the infinite number of such intersections within $\mathcal{N}$ containing the limits

$t \to \pm\infty$). This observation strongly suggests that, disregarding the two tails, the total number of oscillations (i.e. the sum of the symbols of an orbit plus the number of crossings of the u-axis before the first hump and after the last hump, of a truncation of the orbit to a finite interval $t \in [-t_0, t_0]$ such that $u(t_0) \neq 0$) should remain constant along a locus of homoclinic orbits. Note that this property is obeyed by all the rules for coalescence; in rules (5.5),(5.6) and (5.7) the sum of all the symbols is preserved, and in (5.4) the sum is increased by four via two oscillations in the tail growing to become humps.

Consider now the ordering (Definition 3.1) of homoclinic orbits in the unstable manifold. If we accept this ordering then all coalescence must be compatible with it. For example, coalescent pairs $a \leftrightarrow b$ and $c \leftrightarrow d$ would be impossible if $a \prec c \prec b \prec d$, but possible if $a \prec b \prec c \prec d$ or $a \prec c \prec d \prec b$. This raises the question why the coalescence $\mathbf{2}(1) \leftrightarrow \mathbf{4}(2,1,2)$ is possible when $\mathbf{2}(1) \prec 1(\infty) \prec \mathbf{4}(2,1,2)$ if the primary orbit $\mathbf{1}(\infty)$ exists for all $P \in [-2,2]$? The answer lies in the fact that the local unstable manifold, in a neighbourhood of the origin, for $P \in (-2,2)$ is a two-dimensional manifold that is divided into two components, I_0 and I_1 say, by the primary and $\mathbf{2}(2)$ orbits (which numerical calculations suggest to exist for all $P \in (-2,2)$). Specifically, let I_0 be such that it contains all orbits with label σ satisfying $\mathbf{1}(\infty) \prec \sigma \prec \mathbf{2}(2)$, see Figure 28.

Moreover, we have that $\mathbf{2}(1)$ and $\mathbf{4}(2,1,2)$ are in the same component because $\mathbf{2}(1) \prec 1(\infty) \prec \mathbf{2}(2) \prec \mathbf{4}(2,1,2)$. Hence, returning to the hypothetical example above of $a \leftrightarrow b$, $c \leftrightarrow d$ where $a \prec c \prec d \prec b$, it is possible to have that either of the two coalescences occurs for a lower P-value, depending on the positions of a, b, c, d relative to $\mathbf{1}(\infty)$ and $\mathbf{2}(2)$. These remarks yield the following principles:

(P1) *Two symbol sequences in I_0 may form a locus; two symbol sequences in I_1 may form a locus; but a symbol sequence in I_0 may not form a locus with a symbol sequence in I_1.*

(P2) *If two symbol sequences σ_1 and σ_2 in I_0 coalesce when $P = \hat{P}$ and $\sigma_1 \prec \sigma \prec \sigma_2$ then σ must coalesce with another symbol sequence in I_0 at a P-value smaller than $\hat{P}$.*

(P3) *If two symbols τ_1 and τ_2 in I_1 coalesce when $P = \hat{P}$ and $\tau_1 \prec \tau_2 \prec \sigma$, for all $\sigma \in I_0$, then all symbol sequences τ with $\tau_1 \prec \tau \prec \tau_2$ must coalesce with a symbol sequence in I_1 for a P-value smaller than $\hat{P}$.* The same is true of $\sigma \prec \tau_1 \prec \tau_2$, for all $\sigma \in I_0$.

(P4) *Suppose two symbol sequences τ_1 and τ_2 have $\tau_1 \prec \sigma \prec \tau_2$ for all $\sigma \in I_0$ and $\tau_1 \leftrightarrow \tau_2$ coalesce at $P = \hat{P}$. If τ does not lie between τ_1 and τ_2 then τ must coalesce with*

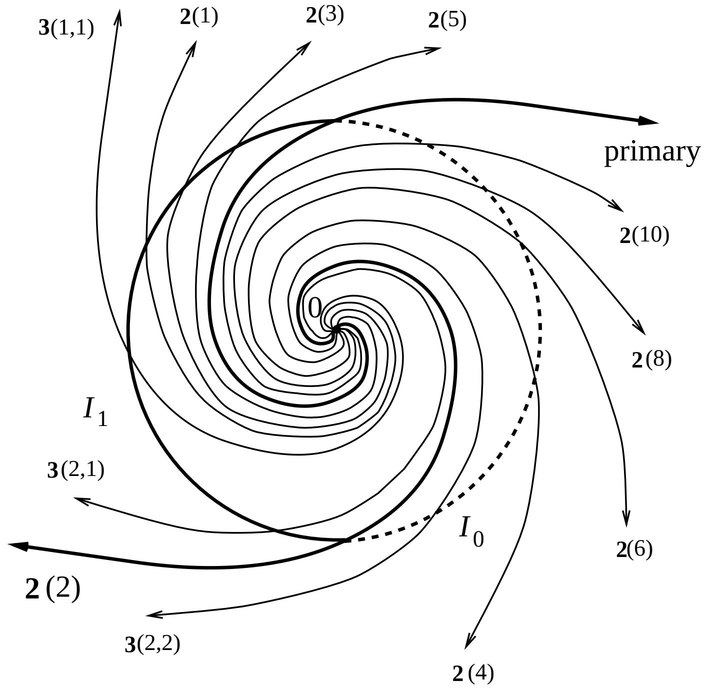

Figure 28: *Schematic diagram of homoclinic orbits in the unstable manifold in a neighbourhood of* 0 *for* $P \in (-2, 2)$, *obeying the ordering defined by Definition 3.1. The dashed and semi-circles represent the two components,* I_0 *and* I_1 *of the set of orbits in the unstable manifold, bounded by the primary and* $\mathbf{2}(2)$ *orbits.*

another symbol sequence in I_1 for a value of P less than $\hat{P}$.

First we shall use these principles to explain the observed ordering with respect to P of certain coalescences computed in Section 5. Recall the observation made from Table 1 that the P-values of coalescence of bi-modal orbits form two eventually increasing sequences, one for orbits with even symbol and one for those with odd symbol. To see why this must be so, assuming that the coalescences occur according to rule (5.1), suppose that for some i, $\mathbf{2}(2i-1) \leftrightarrow \mathbf{4}(2, 2i-1, 2)$ form a locus. Now note the total ordering

$$\mathbf{2}(2i-1) \prec \mathbf{1}(\infty) \prec \mathbf{2}(2) \prec \mathbf{4}(2, 2i-1, 2).$$

It follows that the coalescence of $\mathbf{2}(2i-1)$ with $\mathbf{4}(2, 2i-1, 2)$ occurs in I_1.

Now if $i < j$, then

$$\mathbf{2}(2i-1) \prec \mathbf{2}(2j-1) \prec \mathbf{1}(\infty) \prec \mathbf{2}(2) \prec \mathbf{4}(2, 2j-1, 2) \prec \mathbf{4}(2, 2i-1, 2).$$

Thus if $i < j$ then the coalescence $\mathbf{2}(2i-1) \leftrightarrow \mathbf{4}(2, 2i-1, 2)$ occurs for a smaller P-value than that for $\mathbf{2}(2j-1) \leftrightarrow \mathbf{4}(2, 2i-1, 2)$.

Similarly, if $i < j$, then

$$\mathbf{1}(\infty) \prec \mathbf{2}(2j+2) \prec \mathbf{2}(2i+2) \prec \mathbf{4}(2, 2i-2, 2) \prec \mathbf{4}(2, 2j-2, 2) \prec \mathbf{2}(2).$$

Hence, the coalescence $\mathbf{2}(2j+2) \leftrightarrow \mathbf{4}(2, 2j-2, 2)$ occurs in I_0 at a P-value larger than that at which the coalescence $\mathbf{2}(2i+2) \leftrightarrow 4(2, 2i-2, 2)$ occurs.

Another example of how (P1)–(P4) can determine the ordering of the P-values of certain coalescences is provided by the sequence of orbits $\mathbf{4}(3, i, 3)$ for $i = 3, 4, \ldots \infty$. Suppose that, as observed for a finite number in Table 3, all these orbits coalesce according to the rules (5.4) and (5.5). Recall then the observation from Table 3 and other untabulated data in Section 5.1 that the P-values of the coalescences of the sequences $\mathbf{4}(3, 2j+1, 3)$ and $\mathbf{4}(3, 2j+2, 3)$, $j \in \mathbb{N}$, represent two eventually increasing sequences converging to $P \approx 1.907$ and $P \approx 1.905$ respectively. With reference to Figure 29 notice that all of the coalescences involved occur in I_1. Also with reference to the Figure, notice further that the ordering

$$\mathbf{4}(3, 2j+2, 3) \prec \mathbf{4}(3, 2i+2, 3) \prec \mathbf{6}(3, 2, 2i-2, 2, 3) \prec \mathbf{6}(3, 2, 2j-2, 2, 3) \prec \ldots \prec \mathbf{4}(3, 2, 3)$$

where $i < j$ implies that the coalescence $\mathbf{4}(3, 2i+2, 3) \leftrightarrow \mathbf{6}(3, 2, 2i-2, 2, 3)$ must occur at a lower P-value than $\mathbf{4}(3, 2j+2, 3) \leftrightarrow \mathbf{6}(3, 2, 2j-2, 2, 3)$. Similarly, the ordering

$$\mathbf{6}(2, 3, 2i+1, 3, 2) \prec \mathbf{6}(2, 3, 2j+1, 3, 2) \prec I_0 \prec \mathbf{4}(3, 2j+1, 3) \prec \mathbf{4}(3, 2i+1, 3)$$

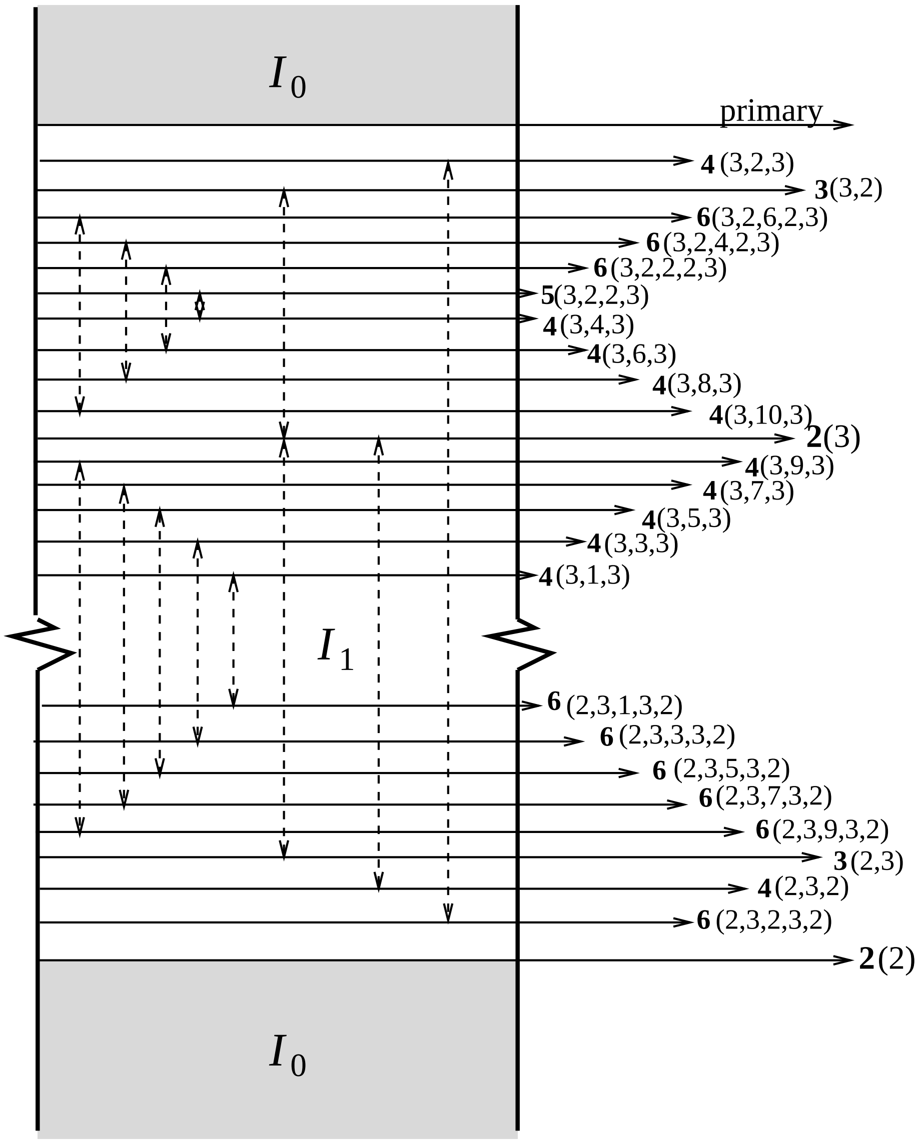

Figure 29: *Illustrating the ordering of homoclinic orbits in I_1 and its consequences on the P-values of coalescence of orbits with labels* $\mathbf{4}(3,*,3)$*. Here, a double arrow indicates orbits that are observed numerically to coalesce (or, in the case of* $\mathbf{3}(2,3)$ *and* $\mathbf{3}(3,2)$*, to bifurcate).*

where $i < j$ implies that the coalescence $\mathbf{4}(3, 2i+1, 3) \leftrightarrow \mathbf{6}(2, 3, 2i+1, 3, 2)$ must occur at a lower P-value than $\mathbf{4}(3, 2j+2, 3) \leftrightarrow \mathbf{6}(3, 2, 2j-2, 2, 3)$ if $i < j$. Hence both of the sequences mentioned above must be increasing. Moreover, they are both bounded since the ordering

$$\mathbf{3}(3,2) \succ \mathbf{6}(3, 2, 2i-2, 2, 3) \succ \mathbf{4}(3, 2i+2, 3) \succ \mathbf{2}(3)$$

implies that all the coalescences $\mathbf{4}(3, 2i+2, 3) \leftrightarrow \mathbf{6}(3, 2, 2i-2, 2, 3)$, $i \in \mathbb{N}$, must occur for lower P-values than the bifurcation of $\mathbf{3}(3, 2)$ from $\mathbf{2}(3)$ (note from Figure 29 that it is impossible for $\mathbf{3}(3, 2)$ to bifurcate from $\mathbf{4}(3, 2, 3)$). Similarly the ordering

$$\mathbf{4}(3, 2i+1, 3) \prec \mathbf{2}(3) \prec I_0 \prec \mathbf{4}(2, 3, 2) \prec \mathbf{6}(2, 3, 2i+1, 3, 2)$$

implies that all the coalescences $\mathbf{4}(3, 2i+1, 3) \leftrightarrow \mathbf{6}(2, 3, 2i+1, 3, 2)$, $i \in \mathbb{N}$, must occur for lower P-values than $\mathbf{2}(3) \leftrightarrow \mathbf{4}(2, 3, 2)$. Note the numerical observations that $\mathbf{3}(2, 3)$ bifurcates at $P = 1.90718$ and $\mathbf{2}(3) \leftrightarrow \mathbf{4}(2, 3, 2)$ occurs at $P = 1.90727$, which bounds are consistent with the numerically observed P-values of the coalescences of the sequences $\{\mathbf{4}(3, 2i+2, 3) | i \in \mathbb{N}\}$ and $\{\mathbf{4}(3, 2i+1, 3) | i \in \mathbb{N}\}$ respectively.

Finally, we consider two examples illustrating how (P1)–(P4) can help determine which rule among alternatives may apply in the two undecided parts of the rules for coalescence discussed in Section 5.1. Consider first the indeterminacy in the rule (5.7). Observe, from Table 3, the coalescences of $\mathbf{4}(6, 1, 6)$ and $\mathbf{4}(6, 2, 6)$. Note that another conceivable situation

$$\mathbf{4}(6, 1, 6) \leftrightarrow \mathbf{6}(2, 4, 1, 4, 2) \quad \text{and} \quad \mathbf{4}(6, 2, 6) \leftrightarrow \mathbf{6}(4, 2, 2, 2, 4)$$

is impossible, due to the ordering

$$\mathbf{4}(6, 2, 6) \prec \mathbf{4}(6, 1, 6) \prec \mathbf{6}(4, 2, 2, 2, 4) \prec \mathbf{6}(2, 4, 1, 4, 2).$$

Second, we look at an example from Table 4 where the smallest changeable symbol is not unique. Specifically, why does $\mathbf{8}(4, 1, 4, 1, 4, 1, 4)$ not coalesce with $\mathbf{10}(2, 2, 1, 4, 1, 4, 1, 2, 2)$? This is because such a coalescence would be incompatible with $\mathbf{4}(4, 1, 4) \leftrightarrow \mathbf{6}(2, 2, 1, 2, 2)$ due to the ordering

$$\mathbf{8}(4, 1, 4, 1, 4, 1, 4) \prec \mathbf{4}(4, 1, 4) \prec \mathbf{10}(2, 2, 1, 4, 1, 4, 1, 2, 2) \prec \mathbf{6}(2, 2, 1, 2, 2,).$$

We end our discussion with the pessimistic conclusion that to prove precisely which pairs of symmetric homoclinic orbits coalesce appears a daunting, perhaps impossible, task. We emphasize that even these painstaking attempts to deduce empirical rules for coalescence from numerical experiments are speculative and will doubtless need further refinement in the light of numerical results on higher-modal orbits not yet considered. Of course, one can never understand properly the rules of coalescence by performing a *finite* number of numerical experiments on the *infinite* number of homoclinic orbits known to exist.

References

AMICK, C.J., & KIRCHGASSNER, K. 1989. A theory of solitary water-waves in the presence of surface tension. *Arch. Rational Mech. Anal.*, **105**.

AMICK, C.J., & TOLAND, J.F. 1991. Points of egress in problems of Hamiltonian dynamics. *Math. Proc. Camb. Phil. Soc.*, **109**, 405–417.

AMICK, C.J., & TOLAND, J.F. 1992. Homoclinic orbits in the dynamic phase space analogy of an elastic strut. *European J. Appl. Maths.*, **3**, 97–114.

BELYAKOV, L.A., & ŠIL'NIKOV, L.P. 1990. Homoclinic Curves and Complex Solitary Waves. *Selecta Mathematic Sovietica*, **9**, 219–228.

BEYN, W.-J. 1990. The numerical computation of connecting orbits in dynamical systems. IMA *J. Num. Anal.*, **9**, 379–405.

BUFFONI, B. 1993a. *Infinitely many large amplitude homoclinic orbits for a class of autonomous Hamiltonian systems.* To appear in *J. Dff. Eqns.*

BUFFONI, B. 1993b. *Periodic and homoclinic orbits for Lorentz-Lagrangian systems via variational methods.* Submitted.

BUFFONI, B., & TOLAND, J.F. *Global existence of homoclinic and periodic orbits for a class of autonomous Hamiltonian systems.* To appear in *J. Diff. Eqns.*

CHAMPNEYS, A.R. 1994. *Subsidiary homoclinic orbits to a saddle-focus for reversible systems.* To appear in *Int. J. Bifurcation & Chaos.*

CHAMPNEYS, A.R., & SPENCE, A. 1993. Hunting for homoclinic orbits in reversible systems: a shooting technique. *Adv. Comp. Math. 1.* In Press.

CHAMPNEYS, A.R., & SPENCE, A. 1994. *The numerical computation of homoclinic orbits in reversible systems.* In preparation.

CHAMPNEYS, A.R., & TOLAND, J.F. 1993. Bifurcation of a plethora of multi-modal homoclinic orbits for autonomous Hamiltonian systems. *Nonlinearity*, **6**, 665–722.

DEVANEY, R.L. 1976. Homoclinic orbits in Hamiltonian systems. *J. Diff. Eqns.*, **21**, 431–438.

DOEDEL, E. 1981. AUTO, a program for the automatic bifurcation analysis of autonomous systems. *Cong. Numer.*, **30**, 265–384.

DOEDEL, E.J., KELLER, H.B., & KERNÉVEZ, J.P. 1991a. Numerical analysis and control of bifurcation problems: (I) Bifurcation in finite dimensions. *Int. J. Bifurcation and Chaos*, **1**, 493–520.

DOEDEL, E.J., KELLER, H.B., & KERNÉVEZ, J.P. 1991b. Numerical analysis and control of bifurcation problems: (II) Bifurcation in infinite dimensions. *Int. J. Bifurcation and Chaos*, **1**, 745–772.

FRIEDMAN, M.J., & DOEDEL, E. 1991. Numerical computation of invariant manifolds connecting fixed points. SIAM *J. Numer. Anal.*, **28**, 789–808.

HOFER, H., & TOLAND, J.F. 1984. Homoclinic, heteroclinic and periodic orbits for a class of indefinite Hamiltonian Systems. *Math. Annalen*, **268**, 387–403.

HUNT, G.W., & WADEE, M.K. 1991. Comparative Lagrangian formulations for localised buckling. *Proc. R. Soc. Lond. A*, **434**, 485–502.

HUNT, G.W., BOLT, H.M., & THOMPSON, J.M.T. 1989. Structural localisation phenomena and the dynamical phase-space analogy. *Proc. R. Soc. Lond. A*, **425**, 245–267.

IOOSS, G., & KIRCHGASSNER, K. 1990. Bifurcation d'ondes solitaires en présence d'une faible tension superficielle. *C. R. Acad. Sci. Paris, Ser. 1*, **311**, 265 –268.

IOOSS, G., & PEROUEME, M.C. 1993. Perturbed homoclinic solutions in reversible 1:1 resonance vector fields. *J. Diff. Eq.*, **102**, 62–88.

KUZNETSOV, Yu.A. 1990. Computation of invariant manifold bifurcations. *Pages 183–195 of:* Roose, D., Spence, A., & De Dier, B. (eds), *Continuation and Bifurcations: Numerical Techniques and Applications.* Dordrecht, Netherlands: Kluwer.

LAU, Y.-T. 1992. The Cocoon Bifurcations in three-dimensional systems with two fixed points. *Int. J. Bifurcation and Chaos*, **2**, 543.

MIELKE, A. 1991. *Personal Communication.* Bath.

TOLAND, J.F. 1986. Existence of symmetric homoclinic orbits for systems of Euler-Lagrange equations. *Proc. Symp. Pure Math.*, **45(2)**, 447–459.

WIGGINS, S. 1988. *Global Bifurcations and Chaos : Analytical Methods.* New York, U.S.A.: Springer-Verlag.